Chem

CellPress
REVIEWS

Review

Surface and Interface Engineering in Copper-Based Bimetallic Materials for Selective CO_2 Electroreduction

Anthony Vasileff,[1,2] Chaochen Xu,[1,2] Yan Jiao,[1] Yao Zheng,[1,*] and Shi-Zhang Qiao[1,*]

The electrochemical CO_2 reduction reaction (CO_2RR) can couple carbon-capture storage with renewable energy to convert CO_2 into chemical feedstocks. For this process, copper is the only metal known to catalyze the CO_2RR to hydrocarbons with adequate efficiency, but it suffers from poor selectivity. Copper bimetallic materials have recently shown an improvement in CO_2RR selectivity compared with that of copper, such that the secondary metal is likely to play an important role in altering inherent adsorption energetics. This review explores the fundamental role of the secondary metal with a focus on how oxygen (O) and hydrogen (H) affinity affect selectivity in bimetallic electrocatalysts. Here, we identify four metal groups categorized by O and H affinities to determine their CO_2RR selectivity trends. By considering experimental and computational studies, we link the effects of extrinsic chemical composition and physical structure to intrinsic intermediate adsorption and reaction pathway selection. After this, we summarize some general trends and propose design strategies for future electrocatalysts.

The Bigger Picture

Global consumption of fossil fuels is driving anthropogenic climate change and depleting reserves. To stem these environmental problems and secure future energy commodities, the electrochemical CO_2 reduction reaction (CO_2RR) presents an ideal solution because it can couple carbon-capture storage technology with renewable energy to convert atmospheric CO_2 into useful chemical feedstocks. Efficient catalysts are required to drive this process with adequate energy efficiency and product selectivity. In this review, we discuss how surface and interfacial engineering can be used as a strategy for designing copper alloy and bimetallic materials for selective CO_2 reduction to CO or hydrocarbons and alcohols.

INTRODUCTION

The world currently relies on fossil fuels for energy production and its chemical industries. However, the burning of fossil fuels releases significant carbon dioxide (CO_2) emissions into the atmosphere, which is considered the primary driver for anthropogenic climate change. CO_2 is a highly stable molecule and is generally inert in most conditions. However, under appropriate cathodic reduction potentials and the assistance of protons in solution, CO_2 can be electrochemically activated and converted via the CO_2 reduction reaction (CO_2RR) to reduced products. The CO_2RR is an elegant route to sustainable fuel and chemicals production when coupled with carbon-capture storage technology and renewable energy sources such as solar radiation. However, this process is kinetically sluggish because of the multiple electron transfer steps and high energy barriers involved. Therefore, efficient electrocatalysts are required to reduce the reaction overpotential and facilitate the kinetics to accomplish commercially significant rates. To date, a wide range of electrocatalysts for the CO_2RR have been reported, and reduction products are highly catalyst specific.[1–6] Copper (Cu) is a unique metal because it is the only metal that can form deep reduction products (i.e., hydrocarbons and alcohols) with acceptable activity and efficiency during the CO_2RR.[7] However, the selectivity of Cu toward a certain product is typically poor, generating many reduction products concurrently, which range from two-electron ($2e^-$) transfer products (e.g., CO and HCOOH) to eight-electron ($8e^-$) transfer products (e.g., CH_4) and above.[8–10] On the microscopic level, the origin of copper's poor selectivity is its moderate binding energy of most reaction intermediates.[6,11,12] Additionally, considering the Sabatier

principle, improving the selectivity of copper is not a simple task given that the adsorption energies of different intermediates scale with one another.[11] Thus, it is extremely difficult to optimize the binding of a specific intermediate without affecting another.

For various heterogeneous catalytic processes, it has been found that the relative metal oxygen (O) and hydrogen (H) affinities play important roles in a catalyst's activity and selectivity by influencing the binding strength of specific reaction intermediates on their surface.[13,14] Toward the electrocatalytic CO_2RR, for metals with higher O affinity but lower H affinity than Cu (such as In, Sn, Hg, and Pb), the *COOH intermediate formed after the first reaction step is weakly bound. Therefore, the primary CO_2 reduction product on these surfaces is HCOOH. Evidence even suggests that the reaction may proceed through an O-bound *OCHO intermediate on these metals.[15] However, metals with lower O and H affinities than Cu (such as Zn, Ag, and Au) can bind *COOH stronger than *CO. Therefore, CO is desorbed as the main product with the formation of *COOH as the potential determining step (PDS).[16] Other metals with both higher O affinity and H affinity than Cu (including Co, Ni, Fe, Ir, and Pt) tend to favor the competitive hydrogen evolution reaction (HER), although small amounts of hydrocarbons and alcohols have been detected on these metal surfaces.[14,17–20]

The grouping of CO_2RR products based on a catalyst's O and H affinities leads to the idea that by alloying with specific O-binding or H-binding sites, Cu-based alloys can be engineered to have one or two active sites with tuned binding energies for key reaction intermediates. As a precedent, introducing a secondary metal to tune the activity of Pt is well documented, particularly for the oxygen reduction reaction (ORR) in fuel cells.[21–23] For the ORR, many Pt alloys show significantly improved activity and stability compared with those of pure Pt.[24,25] Although many factors (strain, ligand effect, etc.) can contribute to altering the electronic structure (i.e., d-band center) of a material, it is likely that they all function to weaken the adsorption of O-bound species on the surface. Accordingly, targeting the key reaction intermediates in this way may also be useful for CO_2RR pathway selection. To be specific, metals with high O affinity are favorable for C-O bond cleavage, whereas metals with high H affinity favor proton transfer and provide protons or hydroxyl groups for hydrogenation.[19] However, considering that the HER is generally highly competitive on metal surfaces, it is necessary to understand how these secondary metal sites affect Cu to be able to predict activity and selectivity. Furthermore, the electronic structure and morphology are almost always different in the bimetallic material compared with copper. This inevitably modifies intermediate binding and is therefore another necessary consideration when evaluating Cu bimetallic catalysts.

In this review, we first briefly provide some background to the CO_2RR process and the fundamental principles that govern the selectivity of copper catalysts. We then introduce the concept of interfacial engineering of copper-based catalysts and review current examples of Cu bimetallic electrocatalysts. Each example is categorized into sections on the basis of the O and H affinities of the secondary metal, and we highlight the effects from the introduced O- and H-binding sites on the selectivity of the Cu bimetallic system. The effects of the secondary metal on the chemical composition, electronic structure, geometry, morphology, and electrocatalytic activity of these bimetallic catalysts are then linked to their intermediate binding energetics. This is done with the aim of interpreting any trends in CO_2RR selectivity that might result from modification of the Cu interface with another metal. To further this, we discuss

[1]School of Chemical Engineering, University of Adelaide, Adelaide, SA 5005, Australia

[2]These authors contributed equally

*Correspondence:
yao.zheng01@adelaide.edu.au (Y.Z.),
s.qiao@adelaide.edu.au (S.-Z.Q.)

https://doi.org/10.1016/j.chempr.2018.05.001

some key examples that combine experimental and computational studies in this field. Finally, we propose some general trends on the basis of these metal groups with strategies for the future design of Cu bimetallic electrocatalysts.

FUNDAMENTAL UNDERSTANDING OF THE CO_2RR

CO_2RR Reaction Mechanism on Cu

Cu has been widely studied as an electrocatalyst for the CO_2RR because of its ability to produce hydrocarbons and alcohols at modest overpotentials.[8,17,26–28] Electrocatalytic CO_2RR on Cu proceeds via multiple electron-proton coupled transfer steps to adsorbed intermediates through multiple pathways. Therefore, it is very non-selective and produces a range of products concurrently. Pioneering work by Hori and coworkers found that on Cu electrodes, generally $2e^-$ products (H_2, CO, HCOOH) are formed at lower overpotentials, whereas higher e^- products (CH_4: $8e^-$ and C_2H_4: $6e^-$) are formed at higher overpotentials (Figure 1A).[17,27,29,30] However, the specific mechanism of the CO_2RR on Cu is surface and condition sensitive,[31,32] and a comprehensive understanding is still lacking. As shown in Figure 1B, the most widely accepted reaction pathway to CH_4 proceeds via the hydrogenation of adsorbed *CO to the *CHO intermediate, which is identified as the PDS.[33,34] Further hydrogenation to *CH_2O and *CH_3O then leads to CH_4 production with the remaining reaction steps being exergonic. Additionally, the hydrogenation of the methyl end of *CH_3O is more readily achieved with solvated protons to produce CH_4 than with hydrogen addition at the oxygen end via co-adsorbed *H to produce CH_3OH. Besides the thermodynamic analysis, the role of kinetics for the reactions on Cu surfaces has also been considered.[35] It was found that CH_4 production through the CHO* intermediate faced a 1.21-eV kinetic barrier at a potential of −1.15 V versus reversible hydrogen electrode (RHE), whereas CH_3OH only needed to overcome 0.15 eV at this potential. Therefore, to explain why CH_4 is predominantly produced experimentally it was proposed that *CO reduction to the *COH intermediate is favored over CHO* (Figure 1C).[36] This *COH intermediate then undergoes further reduction to *C and is then hydrogenated by co-adsorbed *H, as has been proposed previously.[10] This pathway also explains the experimentally observed concurrent production of CH_4 and C_2H_4 as a result of the identification of a common intermediate (*CH_2). After considering the kinetic aspects, some other studies support the route through the *CHO intermediate to *CH_2 via *CHOH, mainly because of the sluggish kinetics involved in the hydrogenation of *CH_3O at the methyl end and other experimental observations.[28,37]

Scaling Relationships

An inherent challenge of the CO_2RR is that the binding of intermediates follows conventional scaling relationships on the basis of the formation of similar surface-adsorbate bonds among different intermediates (e.g., *COOH, *CO, and *COH all involve C-bound intermediates). Given this, the adsorption energy of a certain intermediate cannot be optimally tuned without affecting another.[11,38,39] For example, Figure 1D shows the calculated scaling relationships between various C-bound intermediates in the reaction pathway to CH_4. As previously discussed, the hydrogenation of *CO to *CHO is considered the PDS of this process because it has the highest free-energy change (0.74 eV); the magnitude of this energy change predominantly originates from the weak *CHO binding relative to *CO binding.[39] To reduce this, the surface would have to bind *CHO stronger than *CO. However, this is difficult to realize because of the constraint imposed by conventional scaling relationships.[11] Experimentally, the large overpotentials and poor turnover frequencies for CO_2 reduction to CO on Au and Ag electrodes can also be attributed to the similar weak adsorption of *COOH caused by the linear scaling between *COOH and *CO.[40]

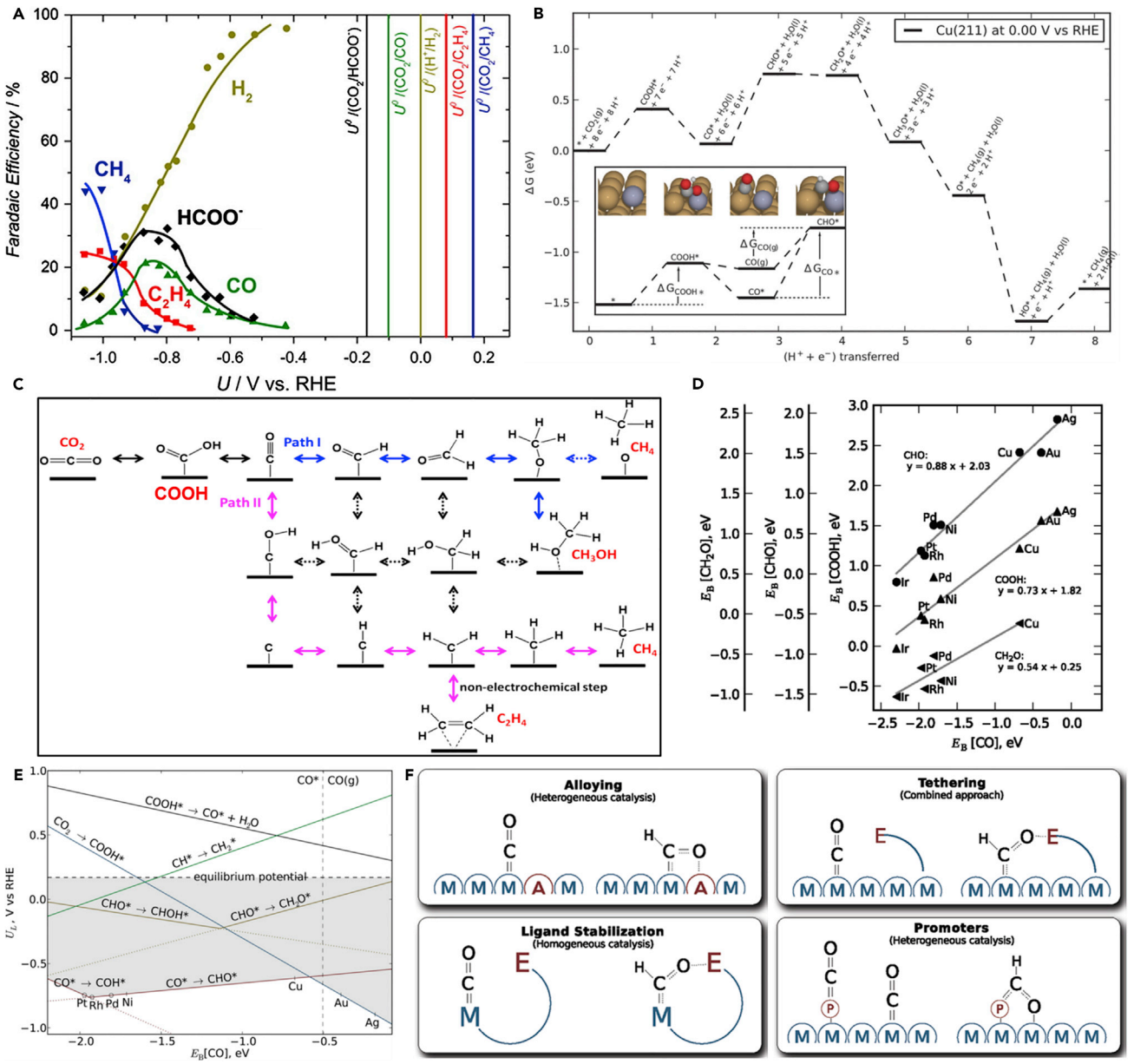

Figure 1. Fundamental Understanding of the CO_2RR on Cu Surfaces

(A) Product distribution expressed as FE as a function of the potential on a polycrystalline Cu electrode. The vertical lines represent the reversible potentials for various products. Adapted from Jovanov et al.[30]

(B) Proposed reaction pathways for the reduction of CO_2 to CH_4 on Cu(211) surface through the *CHO intermediate. Adapted from Hansen et al.[33] with permission of the Royal Society of Chemistry.

(C) The reaction pathway (path II) of the CO_2RR through the *COH intermediate to CH_4, CH_3OH, and C_2H_4. Path I reflects the reaction presented in (B). Adapted from Nie et al.[36]

(D–F) Scaling relationships for C-bound intermediates relevant to the CO_2RR pathway on a range of metal surfaces (D), limiting potentials (U_L) for elementary proton-transfer steps of the mechanism in (B) (E), and suggested decoupling strategies to break these scaling relationships (F). Adapted with permission from Peterson and Norskov.[11] Copyright 2012 American Chemical Society.

Regarding Cu, the fundamental reason for its ability to produce products other than CO at reasonable overpotentials is that it binds *CO neither too weakly nor too strongly (Figure 1B). Therefore, *CO formed on the surface does not desorb immediately (adsorption not too weak), and does not poison the surface (adsorption not

too strong). Furthermore, from Figure 1E it can also be seen that out of all transition metals, Cu has relatively moderate binding of most C-bound intermediate species.[11] As a result, Cu is at the top of the "volcano" plot for the calculated limiting potentials of the two reaction steps which present the largest free-energy barriers (i.e., proton-electron coupled steps: CO_2 to *COOH and *CO to *CHO).[11,37] However, having moderate-level binding of the various surface adsorbates in the pathway also leads to poor selectivity for a particular final product. Therefore, by breaking the above scaling relationships, it is possible to optimize the adsorption energy of a particular intermediate(s) not only for a reduction in overpotential but also for enhanced selectivity. Some useful strategies that focus on tuning the intrinsic electronic parameters underlying the scaling relationships, such as alloying with strong O-binding metals, ligand stabilization, tethering, and addition of promoters, have been proposed (Figure 1F).[11] Ultimately, the aim of these strategies is to strengthen the binding energy of *CHO (i.e., more negative) relative to that of *CO for improved selectivity to deep reduction products.

IMPROVING SELECTIVITY BY INTERFACIAL ENGINEERING

Classification

Various strategies have been employed to enhance the activity of Cu catalysts, and these mainly involve exploiting nanostructuring techniques and morphological control.[9,41–44] However, these approaches generally reduce the overall overpotential for the CO_2RR, improving its selectivity over the HER, and a distinct reduction pathway is not always achieved.[9] With regard to metal catalysts, by coupling two (or more) metal species in alloy or bimetallic materials, the catalyst interface can be engineered to contain multiple sites that contribute to binding of key intermediates in the pathway.[39,45] As a result, designing catalysts on the basis of this principle could lead to conventional scaling relationships being broken in order to tune the selectivity for the reduction of CO_2. Cu is a logical model since it is the only metal catalyst that can promote the CO_2RR toward various hydrocarbon products at non-negligible faradic efficiency (FE).[46] Recently, it has been suggested that alloying Cu, as a form of interfacial engineering, can tune the adjacent chemical environment around the Cu atoms. Therefore, by employing alloys and bimetallic materials, it is possible to tune the binding strength of targeted intermediates on the catalyst surface and enhance the reaction kinetics and selectivity.

In general, the changes to intermediate binding energy, and consequently the reaction pathway, highly depend on the nature of the secondary metal. Herein, we classify the secondary metals on the basis of two factors: H affinity and O affinity; high H affinity describes a metal that binds hydrogen more strongly than Cu, whereas high O affinity describes a metal that binds oxygen more strongly than Cu. The choice of these two descriptors is based on the following considerations. Given that the hydrogenation of *CO is the PDS for deep reduction of CO_2, a secondary site with strong H or O affinity can facilitate the adsorption of *CHO species with alternative configurations (Figure 2A). As a result, the inherent scaling relationship of *CO and *CHO/*COH can be broken. Additionally, the adsorption strength of O-bound reaction intermediates (e.g., *CH_2O and *CH_3O), which appear in the latter half of the CO_2RR pathway, directly relates to the selectivity of hydrocarbon and alcohol products.[47] For determining H and O affinities, a scatterplot presented in Figure 2B provides the trend of H adsorption energy (ΔE_H) against O adsorption energy (ΔE_O) for various metal surfaces. These trends have been extensively used as activity descriptors for the HER and ORR, respectively.[48,49] It can clearly be seen that the metals located to the top left (e.g., Ag and Au) have weaker ΔE_H and ΔE_O than Cu. These

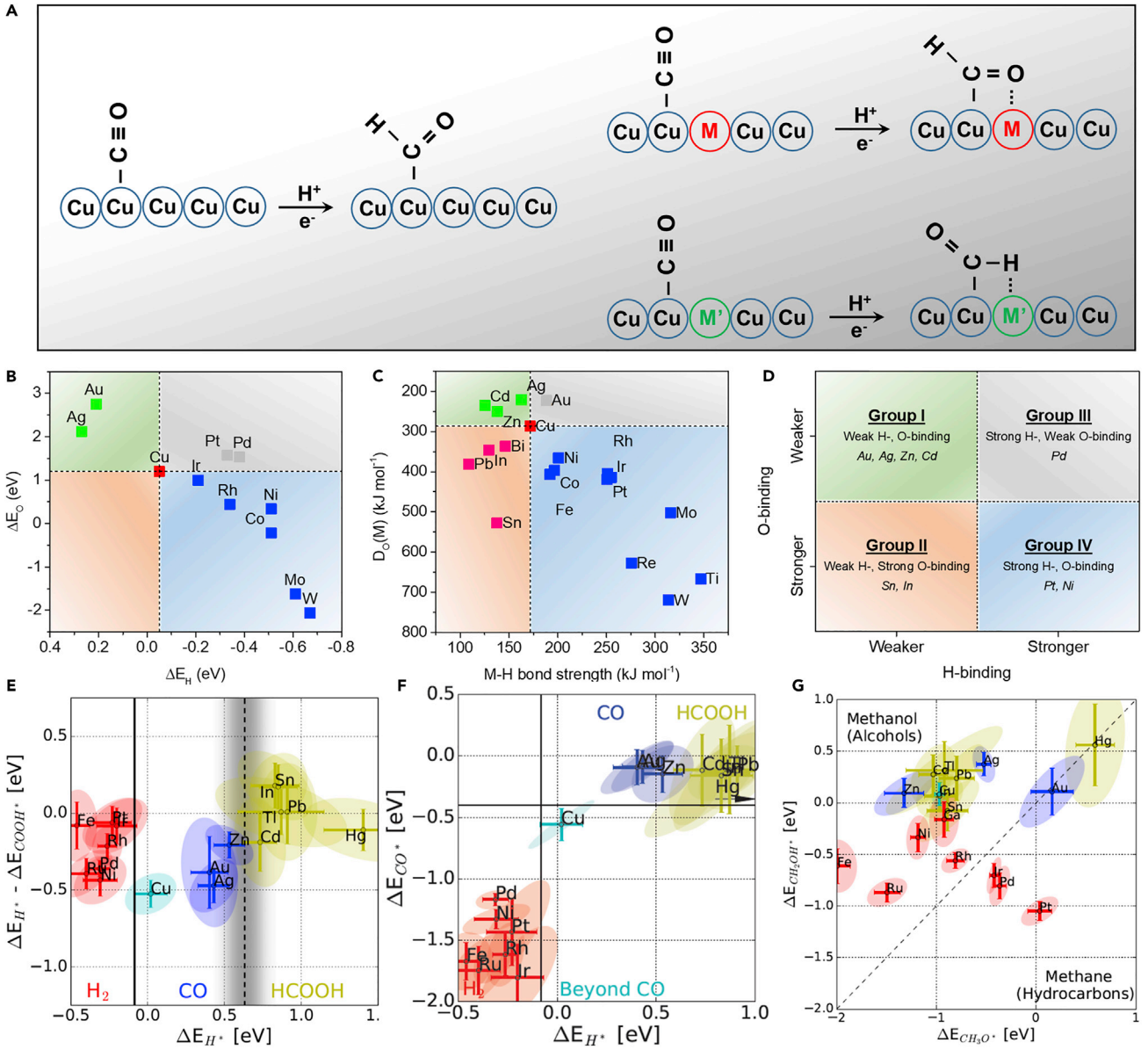

Figure 2. Grouping of Various Metals in Relation to Copper Based on Various Descriptors

(A) Schematic illustration of *CHO adsorption on pure Cu and Cu-M alloy surfaces. M indicates a site with strong O affinity, and M′ indicates a site with strong H affinity.

(B) The oxygen adsorption energy plotted as a function of the hydrogen adsorption energy over different metals. Data of ΔE_O and ΔE_H are from Norskov et al.[48]

(C) The intermediate M-H bond strength plotted as a function of the bond dissociation enthalpy of metal oxides. M-H bond strength data are from Trasatti,[50] and D_O(M) data are from Kepp.[51]

(D) Grouping of various metals in relation to copper alloys based on O and H affinities from previous studies.

(E–G) The experimental product classification of H_2, CO, and HCOOH by the ΔE_{H^*} descriptor (E); the binding energies of intermediates ΔE_{CO^*} and ΔE_{H^*}, which categorize metal catalysts into three distinct groups (F); and the DFT energy relation between ΔE_{CH2OH^*} and ΔE_{CH3O^*} descriptors as a measure of CH_3OH or CH_4 production from carbon-oxygen compounds (G). Adapted with permission from Bagger et al.[6] Copyright 2017 Wiley-VCH Verlag GmbH & Co. KGaA.

metals therefore have to overcome a higher energy to bind hydrogen or oxygen. The metals to the bottom right of Cu (e.g., Ir and Rh) show stronger H and O affinities. The metals located to the top right of Cu (e.g., Pt and Pd) show stronger H affinity

but weaker O affinity. Importantly, these trends can be presented in other forms of H- and O-binding strength. A similar scatterplot shown in Figure 2C provides the trend of the hydrogen-metal bond strength against the enthalpy of bond dissociation of metal oxides as an alternative form. Specifically, for determining H affinity, the strength of the metal-hydrogen (M-H) bond was experimentally measured on various metal surfaces; a greater M-H bond strength favors hydrogen binding.[50] Similarly, a quantitative scale of O affinity has been calculated by applying the enthalpy of bond dissociation for M-O as a descriptor, denoted as D_O(M); metals with D_O(M) values greater than D_O(Cu) signify greater metal-oxygen bond strength (stronger O affinity), and vice versa.[51] As a result, four metal groups are identified depending on their H and O affinity relative to that of Cu (Figure 2D). On the basis of this classification, our goal here is to comprehensively review recent Cu-based alloy (Cu-M) electrocatalysts for the CO_2RR and to evaluate any apparent selectivity trends that may be useful in the rational design of future electrocatalysts.

It should be noted that others have also found that the adsorption energetics of specific reaction intermediates can be applied to classify a wide range of single metals for the CO_2RR. For example, the binding energies of *COOH and *H were calculated as the descriptors to explain the trend of $2e^-$ CO and HCOOH generation for the CO_2RR, whereas binding energies of *CO and *H were applied as the descriptors to predict activity toward deep reduction products.[6] Specifically, as shown in Figure 2E, the metals can be separated into three groups when only ΔE_H is considered as the descriptor: metals with stronger hydrogen affinity than Cu (i.e., within the hydrogen underpotential deposition, H_{upd}, zone) mainly form H_2, metals with moderate H adsorption energy at the CO_2 reduction potential mainly form CO, and metals with weaker H adsorption at the CO_2 reduction potential form HCOOH.[6] Additionally, binding energies of *CO and *H separate Cu from all other metals, as shown in Figure 2F. In this plot, Cu is the only metal in the bottom-right zone possessing relatively weaker *H binding and stronger *CO binding along with the ability to reduce CO_2 to hydrocarbon products or partly reduced alcohol products. It was also found that the C-bound (*CH_2OH) and the O-bound (*CH_3O) intermediates can distinguish hydrocarbon or alcohol formation (Figure 2G). Therefore, four intermediates—ΔE_{H*}, ΔE_{CO*}, ΔE_{COOH*}, and ΔE_{CH3O*}—can be used to explain product groups and selectivity distributions for the CO_2RR on most pure metal surfaces. To predict the products selectivity of Cu-based bimetallic materials, herein we use metal categories based on the O and H affinities of the secondary metal.

Group 1: Weak H Binding and Weak O Binding

Gold (Au)

Au is a d-block metal with both weak hydrogen and oxygen adsorption and has been the most common group 1 metal alloyed with Cu for the CO_2RR. Experimentally it was shown that increased Au content favored CO production, and the pathway to CH_4 was suppressed.[52] Mechanistically, the desorption of CO on Cu sites was promoted because of the lower activation energy for CO desorption caused by Au alloying. In another example, it was found that both the composition and nanostructure of Cu-Au nanoparticles affected the catalytic performance, such that CH_3OH and C_2H_5OH were selectively produced.[53] The optimal $Cu_{63.9}Au_{36.1}$ composition exhibited an FE of 28% for alcohols (including 15.9% for CH_3OH), which is 19 times higher than that of pure Cu. This study claimed that *CO is a significant intermediate for CO_2 reduction toward hydrocarbons and alcohols, whereby binding of *CO was likely optimized in this Cu-Au system. As a comprehensive investigation into the effect of the Cu-Au stoichiometric ratio in bimetallic catalysts,[46] electrochemical results showed that alloys with increased Cu content obtained various reduction

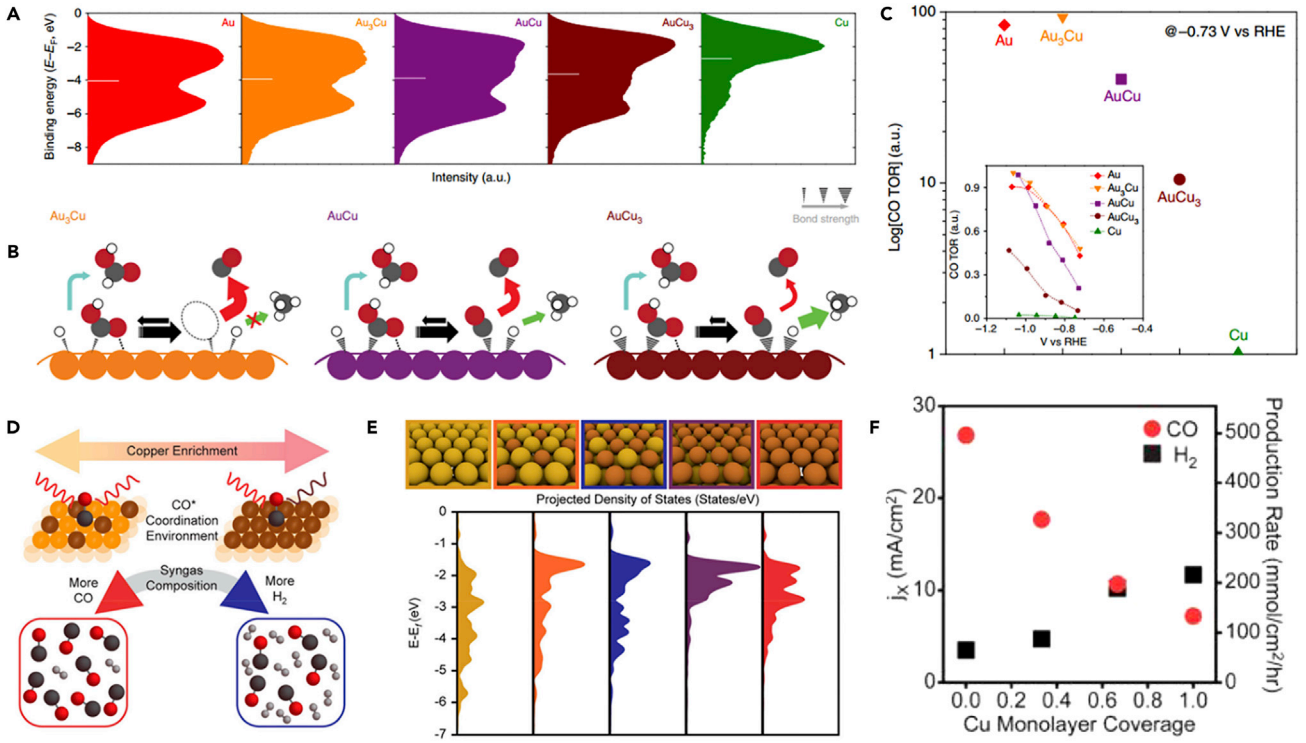

Figure 3. Characterization and Performance of Cu-Au Catalysts for the CO_2RR

(A–C) Surface valence-band photoemission spectra of Au-Cu bimetallic nanoparticles (the white bars indicate the d-band centers) (A); proposed mechanism for the CO_2RR on the surface of Au-Cu bimetallic nanoparticles (gray, red, and white atoms represent C, O, and H, respectively) (B); and CO generation rate on various alloy electrocatalysts at a certain overpotential (inset shows relative CO generation rate as a function of the applied potential) (C). Adapted by permission from Springer Customer Service Centre GmbH: Springer Nature, *Nature Communications*, Kim et al.[46] copyright 2014.

(D–F) Scheme depicting the relationship between the Cu-enriched Au surface, *in situ* characterization of CO* coordination, and syngas composition (D); calculated d-band electronic states for increasingly Cu-enriched Au surfaces (E); and partial current densities (left axis) and production rates (right axis) for CO and H_2 as a function of Cu monolayer deposition on Au (F). Adapted with permission from Ross et al.[55] Copyright 2017 American Chemical Society.

products, whereas increased Au content simultaneously improved CO formation and suppressed other pathways. It was indicated that Cu-Au alloys favored CO production because of their synergistic electronic and geometric effects. Specifically, density functional theory (DFT) calculations demonstrated that the d-band center shifts downwards from pure Cu to pure Au (Figure 3A). As a result, the binding strength for *COOH and *CO should decrease as the Au content increases, and the formation of CO in Cu-Au systems should exhibit a monotonic tendency (Figure 3B). However, *COOH binding was found to be relatively unaffected as a result of an observed geometric effect that stabilized *COOH intermediates. This explains their experimental observations whereby the highest FE toward CO was obtained on Au_3Cu alloy (Figure 3C), and provides a better understanding of the effects of electronic structure and geometric modification in bimetallic materials. Additionally, it was found that increasing the degree of atomic ordering in Cu-Au alloys can tune the selectivity of CO_2 reduction toward CO with a high FE of ~80%, which is due to the stabilization *COOH intermediates on compressively strained Au sites.[54]

Ross et al. used underpotential deposition (UPD) to construct another type of Cu-Au alloy by depositing a single layer of Cu with different coverages (1/3, 2/3, and 1).[55] They found that less Cu coverage increased CO production, whereas increased Cu coverage promoted H_2 evolution. Employing *in situ* Raman microscopy, they used

the vibration of the C-O bond (ν_{C-O}) in *CO species as a descriptor to understand the effects of the Cu/Au ratio on the *CO adsorption strength. It was found that with greater Cu coverage, ν_{C-O} experienced a red shift, which was associated with bond lengthening attributable to greater interaction with the metal (Figure 3D). DFT calculations showed that the projected density of states (DOS) moved further away from the Fermi level on increasingly Au-dominant surfaces, favoring CO production (Figure 3E). On the other hand, Cu enrichment provided a greater improvement to *H adsorption than *CO. Therefore, the degree of Cu enrichment can affect the relative activity of the HER to the CO_2RR, which can realize controllable syngas production (Figure 3F). Similarly, in an Au-Cu core-shell (Au@Cu) system, experimental results indicated that seven to eight layers of Cu resulted in a better selectivity for C_2H_4, whereas CH_4 production slightly increased for 14 or more Cu layers.[56] This was explained by the calculated DFT results, which showed that *COH intermediates were favored over *CHO on terraces; however, *CHO was slightly favored as *CO coverage increased.[57] Therefore, both structural and electronic effects that change the binding of *CO have a significant impact on selectivity and product distribution on the Au@Cu catalysts. In another study, Cu-Au core-shell nanostructures (Cu@Au) also exhibited enhanced current density over polycrystalline Cu and achieved a greater FE toward CO.[58]

Silver (Ag)

Ag is another group 1 metal that has been coupled with Cu for CO_2 reduction. In the Ag-Cu core-shell nanoparticle (Ag@Cu) system, samples with low Cu coverage showed high conversion of CO_2 toward CO, while Cu-dominant nanoparticles had greater selectivity for hydrocarbons.[59] As with the Au@Cu material, both electronic effect and geometric effects were important factors involved in the catalytic activity of the Ag@Cu system. Specifically regarding the electronic effect, the binding energy of *CO on Ag active sites was weaker than that on Cu. Therefore, desorption of CO was facilitated when the coverage of Cu was low. For the geometric effect, the binding strength of intermediates was tuned by changing the local atomic arrangement at the active sites. Additionally, for electrodeposited Cu-Ag alloys, it was found that Cu segregation caused Cu enrichment on the catalyst surface.[60] As a result, the $Ag_{57}Cu_{43}$ alloy achieved 2.2-fold higher mass-normalized activity than the Ag_{100} catalyst. In another study, electrodeposited nanocoral Cu-Ag bimetallic catalysts exhibited only 30% FE toward hydrogen and around 70% for total C_1–C_3 products by a solar-driven electrochemical cell.[61] In this system it appears that Cu contributed the dominant binding effect, as overall product selectivity was poor. However, the Cu-Ag electrode was more active toward producing alcohols and oxygenates compared with pure Cu. Cu-Ag bimetallic catalysts have also been prepared by melting mixtures of Cu and Ag powders with specific atomic ratios.[62] When the Cu content was low, it was found that the Cu was dissolved in the Ag phase and segregated on the surface during the CO_2RR. These Ag-dominant catalysts produced CO as the major product on the surface although the Cu sites formed the reactive sites. On the other hand, the Cu-dominant catalysts suppressed the HER by about 75% without affecting the ability to produce deep reduction products from CO. On the atomic level, it is believed that compressive strain on Cu introduced by neighboring Ag causes a shift in the valence band DOS, therefore causing weaker binding of *H and *O relative to *CO.

Zinc (Zn)

Cu-Zn bimetallic catalysts were also found to be selective toward CO_2 reduction to alcohols, in which Cu_4Zn achieved the highest FE of 29.1%.[63] The authors indicated that CO_2 is reduced to *CO on either Cu or Zn active sites in the first step, and is

further reduced to *CHO or *CH_x (x = 1–3) on the Cu sites. However, because of the weak adsorption of *CO on the Zn sites, desorbed CO may diffuse and spill over on the Cu sites, whereby the *CO can insert between Cu sites and *CH_2 intermediates to form *$COCH_2$, which is then reduced further to produce C_2H_5OH.

Cadmium (Cd)

Hori investigated *in situ* Cd-electrodeposited Cu electrodes under different Cd coverages.[64] At a constant current density, Cd electrodeposition occurred along with the HER and CO_2RR. Therefore, as Cd deposition increased with time, a trend in product selectivity could be observed. The results showed that the FE toward CO increases with increasing Cd coverage, whereas the FE toward other gas products decreases significantly. However, the FE toward CO reaches a maximum, and with further increase in Cd coverage the production of HCOOH is favored.

Group 2: Weak H Binding and Strong O Binding

Tin (Sn)

Sn is identified as a group 2 metal with higher O affinity and weaker H affinity than Cu.[51] Because of its weak H adsorption, Sn metal is relatively inactive toward the HER and Sn electrodes have been found to mainly produce $HCOO^-$.[7,65] This suggests that on Sn, the CO_2RR overwhelmingly proceeds via the *COOH intermediate or, as has been suggested, through the bidentate *OCHO intermediate.[15] In the Cu-Sn bimetallic system, theoretically *CO intermediates are unaffected by O-binding sites (e.g., Sn) as they tend to bind in end-on configurations, where the O atom contributes little to the chemisorption. However, O atoms contribute more in the *COOH intermediate to overall adsorbate stabilization and its binding energy is likely increased when O-binding sites are present.[39] Furthermore, O-binding sites likely play an even greater role if the CO_2RR proceeds via the *OCHO intermediate, as the two oxygens bond to the surface in a bidentate configuration.[15] Cu-Sn bimetallic materials for selective CO_2 reduction have only been demonstrated experimentally in a few cases, and it seems that Sn limits the usual CO_2RR pathway on Cu to $2e^-$ reduction products.[66] For example, it was found that while maintaining an onset potential similar to that of a Cu sheet electrode, a Cu-Sn material was significantly more selective to CO production with an FE of 90% at −0.6 V versus RHE (Figure 4A).[67] In comparison, the Cu sheet achieved a wide range of products (CO, HCOOH, and H_2) under the same conditions (Figure 4B). A noted consequence of coupling Sn with Cu was that the bimetallic material exhibited approximately one-third less catalytic current density compared with the Cu sheet electrode (Figure 4C). However, when considering the improved selectivity for the CO_2RR over the HER on the Cu-Sn material, this difference becomes less significant.

Core-shell Cu-SnO_2 nanoparticles achieved a maximum FE of 93% toward CO at −0.7 V versus RHE for samples with a 0.8-nm thick SnO_2 shell (Figure 4D).[68] In this study, the thickness of the Sn shell was found to have a marked effect on product selectivity. When the shell thickness was increased to 1.8 nm, negligible CO was produced within this range, and instead HCOOH was produced in preference along with increased HER at more positive potentials (Figure 4E). This sample exhibited a trend similar to that in Sn foil, indicating that for increased shell thickness the Sn characteristics dominated the electrocatalytic pathway. DFT calculations found that the 0.8-nm thick SnO_2 shell could induce a large compressive strain on the surface (~10%), and Cu atoms simultaneously diffuse out on the SnO_2 shell. As a result, differing from the 1.8-nm thick SnO_2 shell model on which HCOOH production is energetically more favorable, the overpotential for CO production is less negative than that for HCOOH production on the model where both compression and Cu

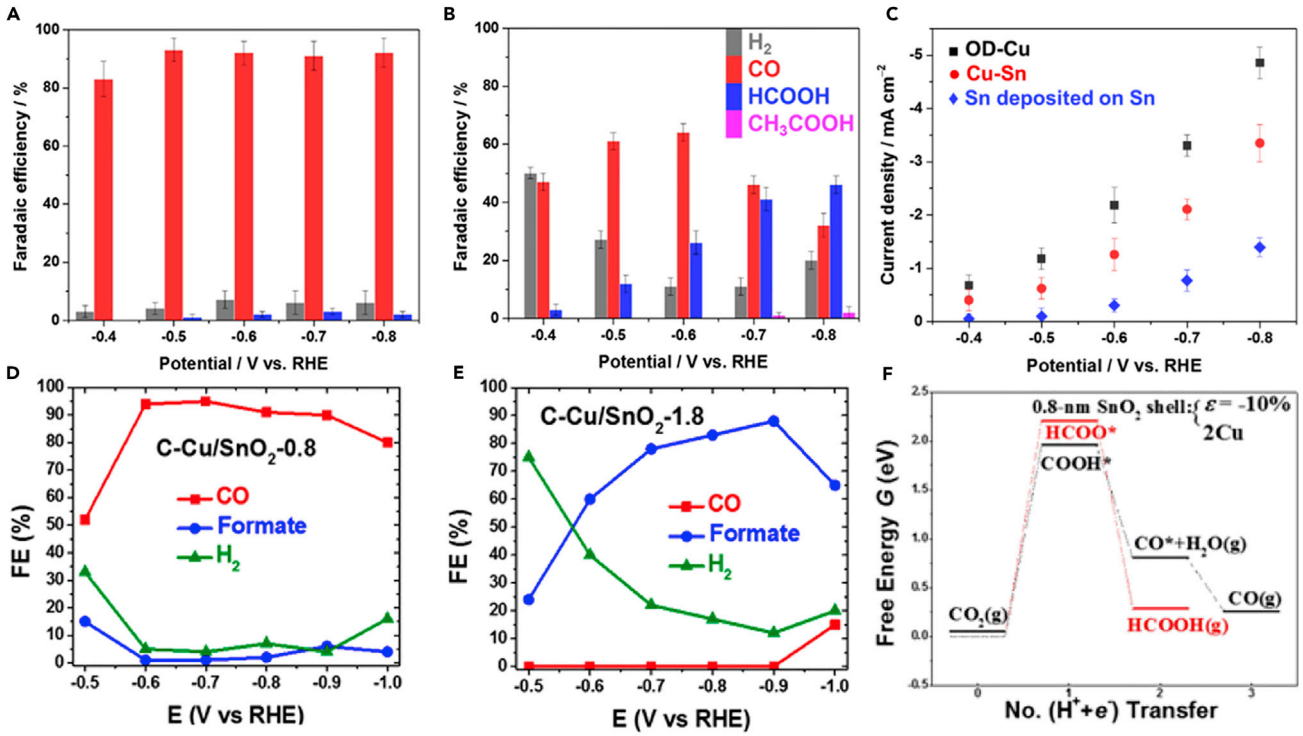

Figure 4. Characterization and Performance of Cu-Sn Catalysts for the CO_2RR

(A–C) FE analysis of (A) Cu-Sn and (B) Cu catalyst at different applied potentials and (C) overall current density of different electrocatalysts. Adapted with permission from Sarfraz et al.[67] Copyright 2016 American Chemical Society.

(D–F) Potential-dependent FEs on different electrodes (D and E) and free-energy diagrams of two reaction pathways on a 0.8-nm SnO_2 shell with two Cu atoms on the surface and 10% uniaxial compression (F). The red and black lines represent the path of HCOOH and CO generation, respectively. Adapted with permission from Li et al.[68] Copyright 2017 American Chemical Society.

doping are present (Figure 4F). Other studies also report the effect of the deposited Sn thickness in Cu-Sn systems, in which the thicker Sn layers favor HCOOH production but thinner layers favor CO production.[66,69] A mechanistic study on SnO_2-coated CuO nanoparticles found that the binding strength of *H and *CO is significantly lower than that of unmodified CuO nanoparticles.[69] As a result, firstly CO will be more easily desorbed from the surface upon formation, and subsequent hydrogenation will be more difficult because of the dilution of adsorbed *H intermediates. Secondly, the weak *H adsorption will limit the HER and increase the selectivity for the CO_2RR. Given that CO is the main product formed on Cu-Sn materials, this view gives a good overall explanation of the underlying mechanism.

Indium (In)

Similarly to Sn, when In was alloyed with Cu the resultant Cu-In electrocatalysts were reported to be highly selective and stable toward CO at low overpotential, reaching FEs of around 90% for CO formation.[45,70] It was found that the presence of In increases the energy barrier to H adsorption but stabilizes the *COOH intermediate by 0.1 eV.[70] As with Sn, binding of *CO was relatively unchanged and the relative increase in stability of *COOH is likely responsible for the observed activity for CO production.

Group 3: Strong H Binding and Weak O Binding

Palladium (Pd)

Pd is identified as a group 3 metal and has been used extensively in the field of gas-phase heterogeneous catalysis.[71,72] Pd has little to no barrier toward H_2 adsorption

and readily forms the metal hydride (PdH_x),[73,74] which makes it a good candidate for catalyzing hydrogenation reactions. As dispersion of Pd atoms on Cu surfaces has been shown to significantly reduce the barrier to hydrogen adsorption, Pd-Cu alloy nanoparticles were employed as heterogeneous catalysts in the hydrogenation of CO_2.[75,76] It was proposed that the stronger binding of *H possibly facilitates this process and affects selectivity toward *COH/*CHO in the CO_2RR.[36] However, pure Pd mainly produces CO during the CO_2RR and only produces small amounts of CH_4, likely because hydride formation inhibits *CO binding.[11] For the Cu-Pd system, alloy composition and intermetallic arrangement were found to have significant effects on activity and selectivity. For example, it was found that Cu-Pd nanoparticles with regular intermetallic arrangements exhibited selective CO_2RR toward CO.[77,78] DFT calculations showed that on an ordered Pd-terminated Pd-Cu (111) surface, binding of *COOH was stronger than Pd (111), and *CO adsorption was significantly weakened. Interestingly, Pd is the active site in this system and the observed effects are the result of neighboring Cu atoms with higher O affinity. Another study explains that the electronic effect of charge transfer from Pd to Cu causes the weaker adsorption of *CO in the Cu-Pd system.[79]

According to d-band theory, a negative shift in the DOS away from the Fermi level normally results in weaker binding of adsorbates on a catalyst surfaces.[80] However, this does not encompass an example of phase-separated Cu-Pd nanoparticles.[81] Therefore, a comprehensive view of intermediate binding is required for catalyst design strategies beyond the d-band center theory. Expanding upon the above example, Cu-Pd bimetallic nanoparticles with various atomic mixing patterns (ordered, disordered, and phase separated) exhibited very different selectivities toward C1 and C2 products (Figures 5A–5C).[81] Specifically, for ordered Cu-Pd nanoparticles the FE toward C1 products (primarily CO) reached approximately 80%. However, for nanoparticles with distinct Cu and Pd phases (phase separated), C2 products (primarily C_2H_4) were selectively produced at an FE of >60%. The underlying reason for this may be that in the phase-separated system, the binding of *CO is less affected when the two sites are segregated. Therefore, Cu sites can facilitate C–C coupling, and co-adsorbed H on Pd sites can facilitate further reduction and hydrogenation of *CO.[75] More importantly, as mentioned above, phase-separated Cu-Pd had the lowest lying d-band center (shown in Figure 5D), and Cu nanoparticles had the highest. This would suggest that the former has the weakest binding and that the latter has the strongest binding of *CO. However, given the experimental results showing that the phase-separated Cu-Pd and Cu nanoparticles have similar catalytic selectivity and activity, geometric and structural effects probably played a more important role than electronic effects in determining catalytic performance among the various Cu-Pd samples.

Cu-Pd nanoparticles have also been applied as photocatalysts for selective CO_2 reduction to CH_4.[82] Nanoparticles with relatively low Cu concentration (Cu/Pd ratio of 1:7) achieved a selectivity toward CH_4 of 96% and effectively suppressed the HER (Figure 5E). The low concentration of Cu in this material was an important factor as it increased the number of isolated Cu atoms in the Pd lattice and, hence, the number of neighboring Cu-Pd sites. On this configuration, as shown in Figure 5F, the CO_2 adsorption energy was maximized at −0.46 eV, which is significantly stronger than on sites with adjacent Cu-Cu atoms (−0.31 eV).[82] Additionally, the Pd atoms had a significant electronic effect on the isolated Cu, causing an increase in their d-band centers and, hence, catalytic activity of the Cu active sites toward multi-electron pathways.

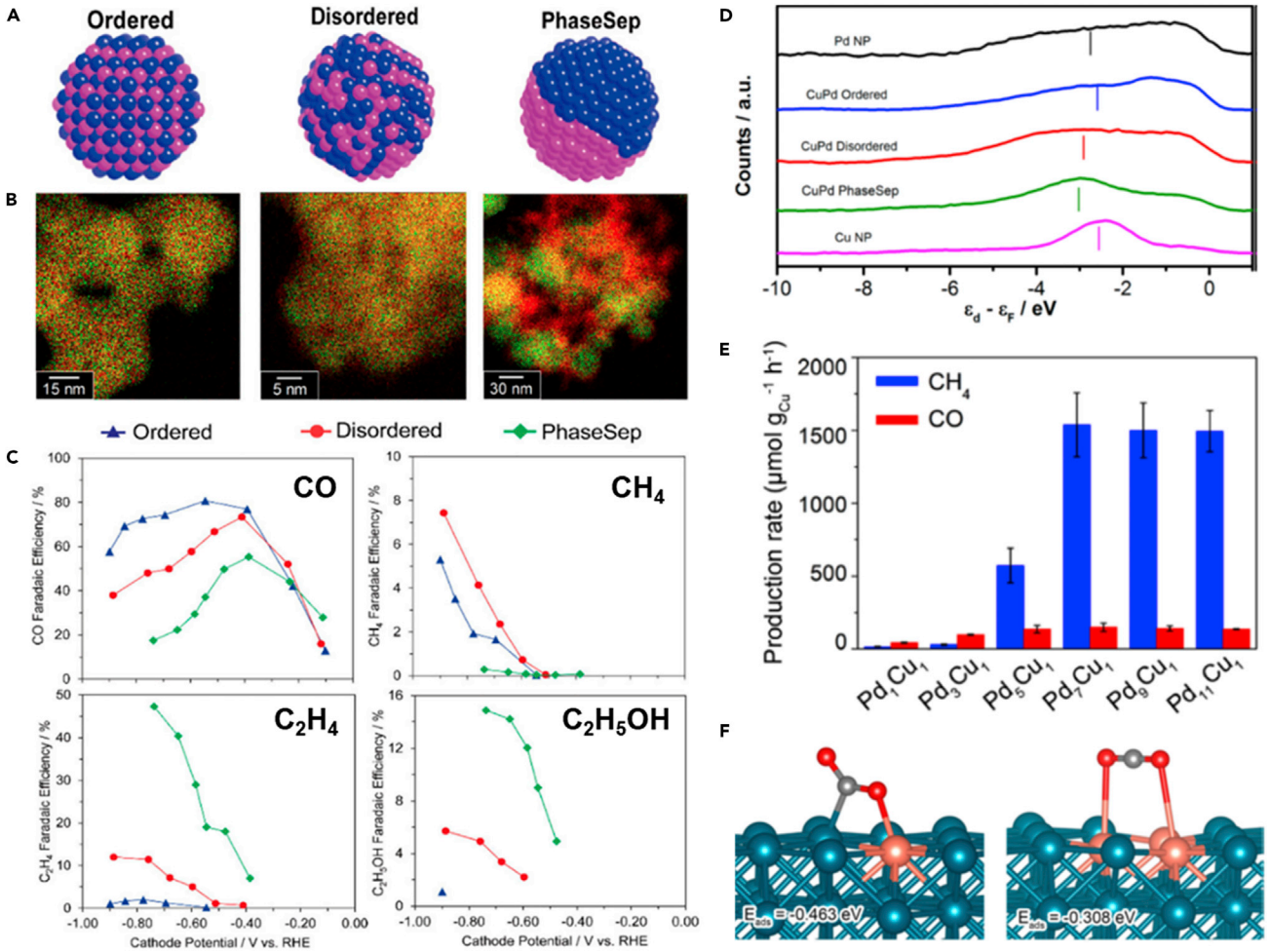

Figure 5. Characterization and Performance of Cu-Pd Catalysts for the CO_2RR

(A–D) Cu-Pd nanoalloys with different atomic mixing patterns (A); combined elemental maps of Cu (red) and Pd (green) (B); FEs for CO, CH_4, C_2H_4, and C_2H_5OH for bimetallic Cu-Pd catalysts with different mixing patterns (ordered [blue], disordered [red], and phase-separated [green]) (C); and background-corrected surface valence-band photoemission spectra of Cu-Pd nanoalloys relative to the Fermi level (the vertical line indicates the d-band center of each sample in relation to the Fermi level) (D). Adapted with permission from Ma et al.[81] Copyright 2017 American Chemical Society. (E and F) Average production rates of CH_4 and CO normalized by the amount of Cu atoms in the Cu-Pd catalysts 9E) and most favorable configurations and adsorption energies of CO_2 at an isolated Cu atom (Cu-Pd pair shown on the left), and two neighboring Cu atoms (Cu-Cu pair shown on the right) (F). Adapted with permission from Long et al.[82] Copyright 2017 American Chemical Society.

Group 4: Strong H Binding and Strong O Binding

Platinum (Pt)

Few examples of group 4 metals being coupled with Cu for CO_2RR electrocatalysts exist in the literature. This is most likely because of their high activity for the competing HER and poisoning by CO. In one study, Varela et al. fabricated Cu UPD layers on Pt (111) and Pt (211) surfaces to study the strain effect on Cu active sites for the CO_2RR.[83] In this study, hydrogen was the major product obtained on Cu/Pt(111) and Cu/Pt(211) samples, as shown in Figure 6A. However, it should be noted that the presence of *CO alters HER activity on the Cu/Pt interface. Specifically, Pt-containing systems are not likely to be stable and can result in Pt segregation because of the strong interaction between Pt and CO. This phenomenon would in turn promote the HER over the CO_2RR. Furthermore, none of the Cu-Pt catalysts could promote CH_4 production as effectively as polycrystalline Cu (Figure 6B). Therefore, this work suggested that the second metal in a Cu bimetallic catalyst

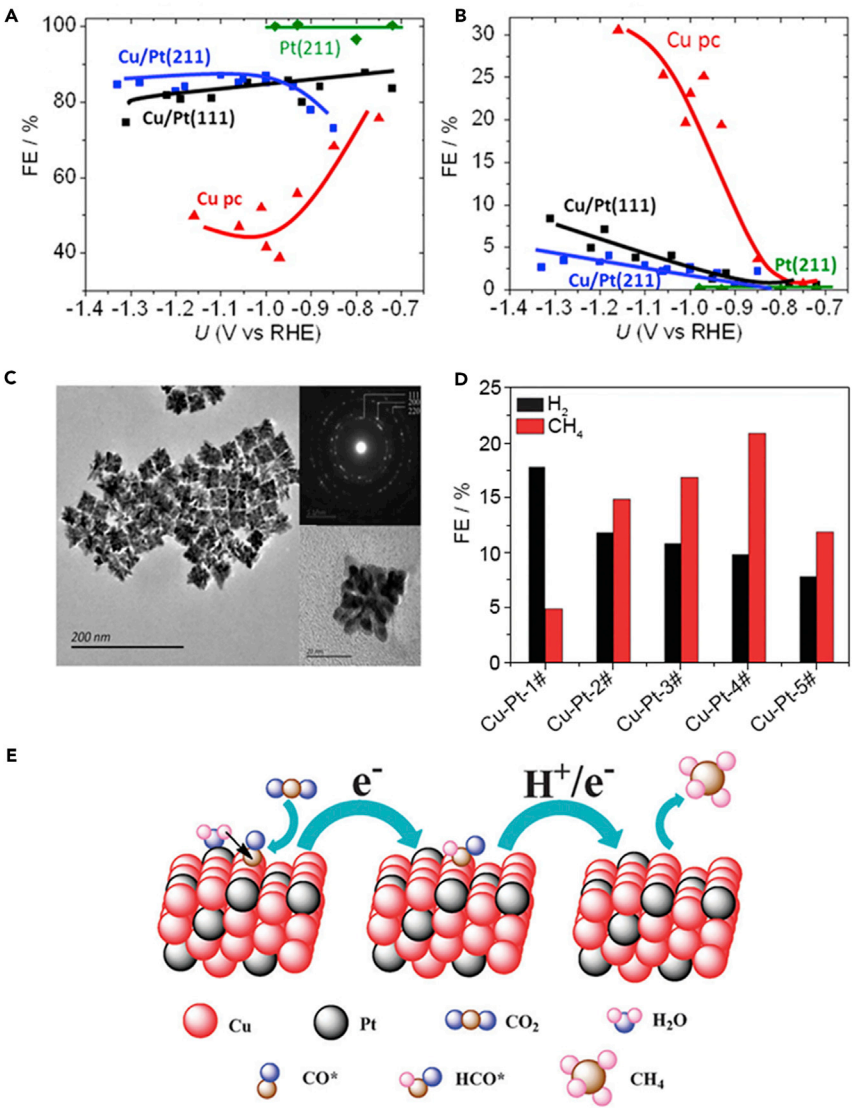

Figure 6. Characterization and Performance of Cu-Pt Catalysts for the CO_2RR

(A and B) FEs toward (A) H_2 and (B) CH_4 as a function of potential on different surfaces. Adapted with permission from Varela et al.[83] Copyright 2013 American Chemical Society.

(C–E) Low-magnification TEM image (scale bar, 200 nm) of the overall morphology of Cu-Pt (inset shows an FFT and high-magnification TEM image [scale bar, 20 nm] of a single Cu-Pt nanocrystal) (C), the FEs of H_2 and CH_4 on different Cu-Pt materials at −1.6 V (D), and a proposed mechanism illustrating the steps of CO_2 electroreduction and CH_4 formation occurring at the Cu-Pt (3:1) catalyst (E). Adapted from Guo et al.[84] with permission of the Royal Society of Chemistry.

should have a lower affinity for *CO. Another study demonstrated that Cu-Pt nanocrystals with controlled Cu/Pt atomic ratios performed with high FE for CH_4 (>20%; Figure 6C).[84] When the Pt content was high, the HER was dominant. With increased Cu content more adsorbed *CO was generated, thereby improving the production of CH_4. However, further increasing the Cu content subsequently led to a higher density of adsorbed *CO and, thus, lower density of adsorbed *H (Figure 6D). Consequently, the overall performance of the alloy was limited as less co-adsorbed H was available to partake in the reaction. On the basis of experimental results, investigation into the possible mechanism showed that increasing the Cu content

increased the surface coverage of *CO on active sites, and Pt facilitated their protonation to *CHO (Figure 6E). However, when insufficient Pt sites are present, *H generation is suppressed and hinders further reduction of *CO.

THEORETICAL PREDICTION

Pathway to CO Production

In recent years, significant advances in computational modeling have made the screening of potential catalysts for various electrochemical processes much easier, including for the CO_2RR.[14,85] Activity trends for a range of metal catalysts and their alloys have also been formulated with activity descriptors, presenting useful predictors for rational catalyst design.[12,33] These trends generally include descriptors based on the PDS of a reaction; for example, binding strength of the *CO intermediate has obvious influence on the rate of CO production. For precious metals such as Pt, although activation and conversion of CO_2 to CO occurs readily, *CO binding is so strong that desorption is the limiting factor and poisons the surface.[12] In contrast, for Au and Ag, which have very weak binding of *CO, experimental studies have shown that they are some of the most selective metals for CO_2 reduction to CO.[7,11,40,86] Furthermore, alloying Au with Cu (Cu having higher O affinity than Au) has shown to be beneficial for the binding strength of the *COOH intermediate, and hence the activity for CO production can be further increased. For example, compared with Au (111) surfaces, it was found that the free-energy change (ΔG) for *COOH formation (ΔG_{*COOH}) decreases on the alloy configurations (Figure 7A).[87] By constructing the Au nanostructures isolated on the Cu surface (Au-*i*@Cu), the ΔG_{*COOH} could be further reduced. In such configurations, the nanostructures increase the number of local under-coordinated sites, which have been shown to increase the binding of intermediates.[86,88] Additionally, corner Au sites adjacent to the Cu surface provide a bifunctional effect for the stabilization of the *COOH intermediate, whereby the high O affinity Cu atoms can stabilize the O end of *COOH (Figure 7B). A similar result was determined on A_3B alloy systems where A = Cu, Au, Ag and B = p-group metals.[33] First, it was found that scaling relationships between *COOH, *CO, and *CHO intermediates on the pure metals limit their activity for reduction of CO_2 to *CO and the reduction of *CO to *CHO and onward. Alloying may preferentially increase the interaction of active sites with *COOH or *CHO, resulting in preferential stabilization of these intermediates over *CO (Figure 7C). In this case, the C end of *COOH tends to bind to the A site, whereas the O end has significant interaction with the B site. As a result, the inherent scaling relationship may be broken. Therefore, an important design principle for alloy materials is the coupling of different metal sites that interact with C-bound and O-bound species differently.

Pathways Beyond CO

It is known that the hydrogenation of *CO to *CHO is generally the PDS in the CO_2RR pathway beyond CO. Therefore, destabilization of the *CO intermediate was found to be crucial in reducing the overpotential for the subsequent protonation steps.[32,33] When O-binding sites are created through alloying, *CO may be forced to bind in an unfavorable configuration, and therefore *CHO will be preferentially stabilized. For example, in the Cu-Ni system, C-bound species were generally found to be better stabilized on Ni (211) facets, whereas binding of O-bound intermediates was not changed significantly compared with Cu (211).[90] Therefore, the Cu_3Ni alloy reflected the difference in intermediate binding between the two parent metals. In a follow-up study, the ligand and strain effect on alloys of Cu with Ni and Rh were investigated.[91] In these systems, a significant reduction in overpotential was achieved on a Cu monolayer deposited on an expanded Ni (211) surface, resulting from the effect of expansive strain on the binding of *CO versus *CHO. For Rh overlayers on Cu, the

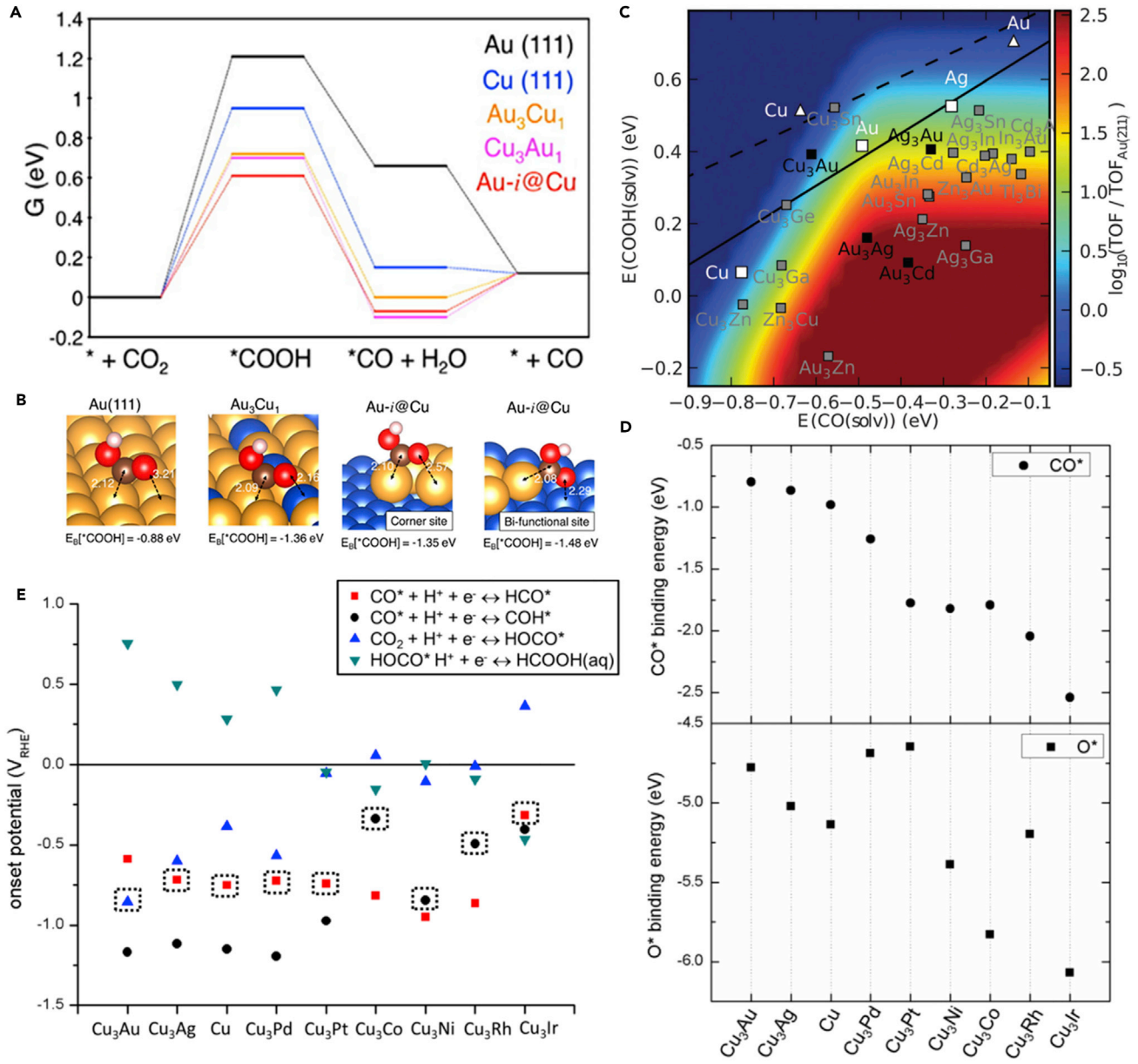

Figure 7. Computational Studies of Various Cu-Based Alloy Catalysts for the CO_2RR

(A and B) Free-energy diagrams for CO generation on various Cu-Au surfaces (A) and binding configurations of *COOH on Au(111), Au_3Cu_1(111), and a corner and bifunctional site of Au-i@Cu (yellow, blue, black, red, and white atoms indicate Au, Cu, C, O, and H, respectively) (B). Adapted with permission from Back et al. [87] Copyright 2016 American Chemical Society.

(C) Breaking the scaling relationship between *COOH and *CO on various alloy surfaces. Color bar indicates CO production on (211) steps normalized to the rate on Au(211). Alloys unstable against corrosion at 0 V versus RHE and pH 7 are shown in gray. Adapted from Hansen et al.[33] with permission of the Royal Society of Chemistry.

(D and E) *CO and *O binding energies on a range of Cu_3M alloy surfaces (D) and onset potentials of the CO_2, *COOH, and *CO protonation steps on a range of Cu_3M alloy surfaces (the dotted squares indicate the calculated limiting potential step) (E). Adapted with permission from Hirunsit et al.[89] Copyright 2015 American Chemical Society.

Cu was found to experience a tensile strain, which also led to a reduction in *CO binding, and consequently a reduction in the overpotential to CH_4 formation was achieved. In a comprehensive study, CO_2 reduction to CH_4 and CH_3OH on a range of Cu_3M (where M = Au, Ag, Pd, Pt, Ni, Co, Rh, and Ir) alloy surfaces was predicted by

DFT modeling.[89] Generally on these alloys, CH_4 generation was found to be more favorable compared with pure Cu, except for Cu_3Pd and Cu_3Pt, which favored a pathway to CH_3OH. Additionally, the protonation of CO* to HCO* or COH* was the PDS on most surfaces. Of note here, binding of *CO, *O, and *H species was analyzed in detail to reveal the inherent trend of the various surfaces. It was found that *CO and *O binding on the alloy surfaces exhibits a general trend similar to that of the pure secondary metal surfaces. For example, alloying Cu with metals that have weaker O* adsorption than Cu (Ag, Au, Pd, and Pt) continue to have relatively weaker O* adsorption, and vice versa, for the metals with stronger *O adsorption (Ni, Co, Rh, and Ir; Figure 7D). This principle is important for the design of Cu-based bimetallic catalysts from both fundamental and functional perspectives. As shown in Figure 7E, the overpotentials on Cu_3Co, Cu_3Rh, and Cu_3Ir surfaces are lower than that on pure Cu, whereas those on Cu_3Ag, Cu_3Pd, and Cu_3Pt surfaces are similar to that on Cu with the same PDS. Additionally, all Cu_3M alloys increased the binding strength of both *CO and *H, except for Au and Ag. Interestingly, these calculations reveal that the activity on Cu-based alloy catalysts does not show a volcano-type relation as was previously found on pure metal catalysts.

GENERAL TRENDS

On the basis of the above examples, it has been shown that by coupling different metals together, the catalyst surface or interface can be engineered to contain multiple sites that contribute to the binding of key reaction intermediates. We posit that the O and H affinities of these secondary sites are significant in this regard, and rational design strategies can be developed by understanding how they affect intermediate binding during the CO_2RR. Despite the effects of the secondary metal sites, different experimental conditions may also affect CO_2RR activity and selectivity, and these considerations have been investigated in recent studies.[92–94] Therefore, a summary of the Cu-based bimetallic catalysts presented in this review along with their reaction conditions are presented in Table 1 for comparison. In our analysis, we found that when group 1 metals (M_1) are the dominant metal in Cu-M_1 systems, CO is the major product formed and FE is generally better than that of the parent metals.[46,54,59,62] This is most likely because the higher O affinity of Cu increases *COOH stabilization, whereas the weak *CO-binding ability of M_1 metals assists in CO product desorption. Furthermore, the weak H binding also suppresses the HER, which increases the selectivity toward the CO_2RR overall. For group 2 metals (M_2), the apparent trend shows that the selectivity toward $2e^-$ products is favored in Cu-M_2 systems; pathways beyond CO are also most likely suppressed because of weak H binding. When M_2 provides the dominant contribution to the active sites, it is found that HCOOH is the major reduction product.[66,68,69] As the result of an increased number of available O-binding sites, *OCHO may be better stabilized and a pathway to HCOOH through this intermediate may be favored in these systems.[15] However, when M_2 provides a moderate contribution in these systems, CO is generally produced at very high FE.[45,67,68,70] By introducing these O-binding sites next to Cu active sites, it is likely that *COOH is better stabilized than *CO, reducing the barrier to CO formation. Limited studies exist on coupling group 3 metals (M_3; Pd specifically) with Cu, in which the intermetallic arrangement of these materials had a significant impact on the product selectivity. When the metallic arrangement was more regular, CO was the major product and was produced with high FE.[77,81] As with Cu-M_1 systems, it is possible that the higher O affinity of the Cu sites increases *COOH stabilization and reduces the barrier to CO formation. For phase-separated Cu-Pd nanoparticles, C2 products were selectively produced

Table 1. Performance Summary of Recent Reports on Cu-M Alloy and Bimetallic Materials

	Catalyst		Electrolyte	Applied Potential	Highlighted Products with FE	Reference
Group 1	Au	Cu@Au	0.5 M $KHCO_3$	−0.65 V versus RHE	CO (~30%)	Chen et al.[58]
		$Au_{50}Cu_{50}$	PBS	−1.9 V versus Ag/AgCl	carbon-containing products (20% ± 5%)	Christophe et al.[52]
		$Cu_{63.9}Au_{36.1}$/NCF	0.5 M $KHCO_3$	−1.1 V versus SCE	CH_3OH (15.9%), C_2H_5OH (12%)	Jia et al.[53]
		Au_3Cu	0.1 M $KHCO_3$	−0.73 V versus RHE	CO (~65%), $HCOO^-$ (~3%)	Kim et al.[46]
		o-AuCu	0.1 M $KHCO_3$	−0.77 V versus RHE	CO (~80%)	Kim et al.[54]
		Au@Cu1 Au@Cu3	PBS	−0.6 V versus RHE	C_2H_4 (distribution ~20%) CH_4 (distribution ~20%)	Monzo et al.[56]
		1/3 Cu UPD Au	0.1 M $KHCO_3$	−0.55 V versus RHE	CO (~75%)	Ross et al.[55]
		Au_3Cu alloy nanocrystals	0.1 M PBS	−1.6 V versus Ag/AgCl	CH_4 (~35%), CO (~25%), $HCOO^-$ (~8%)	Zhao et al.[95]
	Ag	Ag@Cu-7 Ag@Cu-20	0.1 M $KHCO_3$	−1.06 V versus RHE	CO (82%) C_2H_4 (28.6%)	Chang et al.[59]
		$Ag_{57}Cu_{43}$	0.5 M $KHCO_3$	−1.5 V versus SCE	CO (~40%)	Choi et al.[60]
		CuAg surface alloys	0.05 M Cs_2CO_3		CO dominant (low at % Cu) H_2 and C_2H_4 dominant (high at % Cu)	Clark et al.[62]
		Nanocoral Cu-Ag	0.2 M $CsHCO_3$	−1.0 V versus RHE	C_2H_4 (20%), H_2 (30%–35%)	Gurudayal et al.[61]
	Zn	Oxide-derived Cu_4Zn	0.1 M $KHCO_3$	−1.05 V versus RHE	C_2H_5OH (29.1%), C_2H_4 (~10%)	Ren et al.[63]
	Cd	Cu modified with Cd	0.1 M $KHCO_3$	~−1.66 V versus SHE ~−1.62 V versus SHE	CO (~60%) CH_4 (~40%)	Hori et al.[64]
Group 2	Sn	Cu@SnO_2-0.8 Cu@SnO_2-1.8	0.5 M $KHCO_3$	−0.7 V versus RHE −0.9 V versus RHE	CO (93%) $HCOO^-$ (85%)	Li et al.[68]
		Sn-electrodeposited OD-Cu	0.1 M $KHCO_3$	−0.6 V versus RHE	CO (>~90%)	Sarfraz et al.[67]
		$Cu_{87}Sn_{13}$ $Cu_{55}Sn_{45}$	0.1 M $KHCO_3$	−0.99 V versus RHE −1.09 V versus RHE	CO (60%) $HCOO^-$ (89.5%)	Morimoto et al.[66]
	In	Cu-In alloy	0.1 M $KHCO_3$	−0.5 V versus RHE	CO (90%)	Rasul et al.[70]
Group 3	Pd	Pd-decorated Cu	0.5 M $KHCO_3$	−0.96 V versus RHE	CH_4 (46%–40%), C_2H_4 (7–11%)	Weng et al.[96]
		Disordered CuPd	1 M KOH	−0.89 V versus RHE	CH_4 (~7.5%)	Ma et al.[81]
		PhaseSep CuPd	1 M KOH	−0.74 V versus RHE	C2 chemicals (~65%)	Ma et al.[81]
		$CuPd_3$	1 M KOH	−0.55 V versus RHE	CO (~90%)	Ma et al.[81]
		Pd_7Cu_3	0.1 M $KHCO_3$	−0.8 V versus RHE	CO (~80%)	Li et al.[77]
		Pd_7Cu_3	0.1 M $KHCO_3$	Bias −1.2 V	CO (~75%)	Li et al.[78]
		CuPd nanoalloy (Cu_2Pd)	0.1 M $KHCO_3$	−1.8 V versus Ag/$AgNO_3$	CH_4 (~51%)	Zhang et al.[97]
		Cu_2O-derived Cu with $PdCl_2$	0.1 M $KHCO_3$	−1.0 V versus RHE	C_2H_6 (30.1%), C_2H_4 (3.4%)	Chen et al.[98]
Group 4	Pt	Cu-Pt (at. 3:1) nanocrystal	0.5 M $KHCO_3$	−1.6 V versus SCE	CH_4 (21%)	Guo et al.[84]
		Cu/Pt(111)	0.1 M $KHCO_3$	−1.3 V versus RHE	CH_4 (~7.5%)	Varela et al.[83]
	Ni	Cu-electrodeposited Ni	0.5 M $KHCO_3$ water/MeOH solution	−1.9 V versus Ag QRE	CH_4 (20.2%), C_2H_4 (7.5%)	Kaneco et al.[99]

QRE, quasi-reference electrode; RHE, reversible hydrogen electrode; SCE, saturated calomel electrode.

because the neighboring Cu sites most likely facilitate C–C coupling, whereas spillover of H from Pd sites facilitates hydrogenation.[75] Fewer examples of group 4 metals (M_4) being coupled with Cu exist in the literature. Although M_4 metals with high CO affinity should be avoided, it is interesting that these materials can produce hydrocarbons at relatively high FE.

CONCLUSION AND OUTLOOK

Design and fabrication of selective Cu-based CO_2RR electrocatalysts, especially ones selective for hydrocarbon production, remains a difficult task because of the relatively strong binding of the *CO intermediate during reaction. Surface and interface engineering through coupling Cu with a secondary metal has shown to be a successful initial strategy for reducing the reaction energy barrier to increase its activity. It has also shown to be successful in breaking the scaling relationship that exists between *COOH, *CO, and *CHO/*COH to improve the selectivity of Cu. Here, we have reviewed recent examples of Cu-based alloy and bimetallic materials and how the O and H affinities of the secondary metal affect selectivity. Overall, many examples show that the selectivity for CO/HCOOH and hydrocarbons and alcohols in Cu-M systems can be rationally tuned by modifying O- and/or H-adsorbing sites on the surface. The relationship between an alloy's chemical composition and its CO_2RR activity and selectivity are systematically linked to its intrinsic intermediate binding energies. Along with some general trends, possible design strategies for future CO_2RR electrocatalysts are provided.

The ultimate goal in this field is to design catalysts selective for deep reduction products with high energy density. Therefore, it is crucial that the catalyst design address the inherent scaling between *CO and *CHO intermediates. In some cases, it has been shown that the electronic characteristics of both parent metals are relatively preserved after alloying.[87] For these systems, the binding behavior of the pure metals can be used to predict intermediate binding on the resultant material. Therefore, one such strategy that could be implemented is the limited growth or metal doping of a secondary metal on a Cu surface. This could be achieved by constructing single-metal atom catalysts (SMACs) supported on a Cu substrate. M_3 or M_4 SMAC sites can facilitate hydrogenation of *CO to deeper products while limiting the HER. Additionally, bimetallic dimers of Cu and a secondary metal could exhibit strong interfacial coupling, which could enhance the selectivity for hydrocarbons as has been shown theoretically for M_4 metals.[100] Although Cu-M_3 alloys have shown the best performance toward hydrocarbon production, limited studies exist for these cases. Therefore, more group 3 metals should be identified and studied. Further, ternary alloys with Cu should be explored given that combining specific O-adsorbing and H-adsorbing (i.e., M_2 and M_3) sites next to Cu could also prove beneficial for stabilizing and hydrogenating *CO to deeper products. In all these strategies, greater effort should also be focused on exposing more under-coordinated sites, e.g., steps and corner sites, to maximize the interfacial coupling of different active sites in these materials for optimized binding of intermediates.

To this end, we have provided a general view of the role that O-binding and H-binding sites play at the interface, as well as how they affect the binding of reaction intermediates. Nevertheless, a more profound basis for intermediate energetics is still required. From a theoretical perspective, computational electrochemistry remains the most direct and powerful tool to reveal the microscopic picture of the CO_2RR on different catalyst surfaces. For example, it was identified by computations that the first protonation step (i.e., CO_2 to *COOH) is the step that determines CO_2 activation in the CO_2RR pathway, whereas the second protonation step (i.e., *CO to *COH or *CHO) dominates the selectivity toward different products. Furthermore, electronic structure computation can reveal and direct the subatomic-level and atomic-level tuning of catalyst surfaces. Additionally, the effects of steps, terraces, islands, and single atom morphologies toward the CO_2RR can be visualized directly through computations. However, models used in DFT calculations are normally

constrained to ideal and flat repeating units (this is natural when periodic boundary conditions are adopted). On some catalyst surfaces, it remains a challenge to effectively identify the real active site(s) because of the complexity involved in materials that contain multiple structural features. In some cases, the opposite trend was found to occur on the actual alloy material, whereby instability of the surface can lead to morphological changes during reaction conditions.[30] Therefore, the chemical composition and physical structure stabilities of bimetallic catalysts is a significant consideration and should also be experimentally studied both during and after the CO_2RR process (e.g., surface segregation might be an issue). In the future, more advanced calculations, including high-throughput computation and machine-learning techniques, could be adopted to produce more representative models of these complex catalyst surfaces. Coupled with experimental studies, a route to rational design strategies for CO_2RR electrocatalysts appears possible. The concepts proposed in this review related to O and H affinities are also very general and could be extended to other catalytic processes involving multiple reaction intermediates. Therefore, this general guidance could be adopted for the design of electrocatalysts and heterogeneous catalysts for the ORR, alkaline HER, CO_2 hydrogenation, and so forth.

ACKNOWLEDGMENTS

The authors gratefully acknowledge financial support from the Australian Research Council through the Discovery Project programs (DP160104866, DP170104464, DE160101163, and FL170100154) and the Linkage Project program (LP160100927) and the Australian Government through Research Training Program Scholarships.

AUTHOR CONTRIBUTIONS

All authors devised the concept and built the framework of the review. A.V. and C. X. wrote the manuscript and organized the figures. Y.J., Y.Z., and S.-Z.Q. edited and reviewed the manuscript.

REFERENCES AND NOTES

1. Liu, J.L., Guo, C.X., Vasileff, A., and Qiao, S.Z. (2017). Nanostructured 2D materials: prospective catalysts for electrochemical CO_2 reduction. Small Methods *1*, 1600006.

2. Wang, Y., Liu, J., Wang, Y., Al-Enizi, A.M., and Zheng, G. (2017). Tuning of CO_2 reduction selectivity on metal electrocatalysts. Small *13*, 1701809.

3. Zhang, W., Hu, Y., Ma, L., Zhu, G., Wang, Y., Xue, X., Chen, R., Yang, S., and Jin, Z. (2017). Progress and perspective of electrocatalytic CO_2 reduction for renewable carbonaceous fuels and chemicals. Adv. Sci. *5*, 1700275.

4. Zhu, D.D., Liu, J.L., and Qiao, S.Z. (2016). Recent advances in inorganic heterogeneous electrocatalysts for reduction of carbon dioxide. Adv. Mater. *28*, 3423–3452.

5. Vasileff, A., Zheng, Y., and Qiao, S.Z. (2017). Carbon solving carbon's problems: recent progress of nanostructured carbon-based catalysts for the electrochemical reduction of CO_2. Adv. Energy Mater. *7*, 1700759.

6. Bagger, A., Ju, W., Varela, A.S., Strasser, P., and Rossmeisl, J. (2017). Electrochemical CO_2 reduction: a classification problem. ChemPhysChem *18*, 3266–3273.

7. Hori, Y., Wakebe, H., Tsukamoto, T., and Koga, O. (1994). Electrocatalytic process of CO selectivity in electrochemical reduction of CO_2 at metal electrodes in aqueous media. Electrochim. Acta *39*, 1833–1839.

8. Kuhl, K.P., Cave, E.R., Abram, D.N., and Jaramillo, T.F. (2012). New insights into the electrochemical reduction of carbon dioxide on metallic copper surfaces. Energy Environ. Sci. *5*, 7050–7059.

9. Kim, D., Kley, C.S., Li, Y., and Yang, P. (2017). Copper nanoparticle ensembles for selective electroreduction of CO_2 to C_2-C_3 products. Proc. Natl. Acad. Sci. USA *114*, 10560–10565.

10. Hori, Y., Takahashi, R., Yoshinami, Y., and Murata, A. (1997). Electrochemical reduction of CO at a copper electrode. J. Phys. Chem. B *101*, 7075–7081.

11. Peterson, A.A., and Norskov, J.K. (2012). Activity descriptors for CO_2 electroreduction to methane on transition-metal catalysts. J. Phys. Chem. Lett. *3*, 251–258.

12. Hansen, H.A., Varley, J.B., Peterson, A.A., and Norskov, J.K. (2013). Understanding trends in the electrocatalytic activity of metals and enzymes for CO_2 reduction to CO. J. Phys. Chem. Lett. *4*, 388–392.

13. Norskov, J.K., Abild-Pedersen, F., Studt, F., and Bligaard, T. (2011). Density functional theory in surface chemistry and catalysis. Proc. Natl. Acad. Sci. USA *108*, 937–943.

14. Greeley, J., Jaramillo, T.F., Bonde, J., Chorkendorff, I.B., and Norskov, J.K. (2006). Computational high-throughput screening of electrocatalytic materials for hydrogen evolution. Nat. Mater. *5*, 909–913.

15. Feaster, J.T., Shi, C., Cave, E.R., Hatsukade, T., Abram, D.N., Kuhl, K.P., Hahn, C., Nørskov, J.K., and Jaramillo, T.F. (2017). Understanding selectivity for the electrochemical reduction of carbon dioxide to formic acid and carbon monoxide on metal electrodes. ACS Catal. *7*, 4822–4827.

16. Jones, J.P., Prakash, G.K.S., and Olah, G.A. (2014). Electrochemical CO_2 reduction: recent advances and current trends. Isr. J. Chem. *54*, 1451–1466.

17. Hori, Y., Kikuchi, K., and Suzuki, S. (1985). Production of CO and CH_4 in electrochemical reduction of CO_2 at metal electrodes in aqueous hydrogen carbonate solution. Chem. Lett. *14*, 1695–1698.

18. Hori, Y. (2016). CO_2 reduction using electrochemical approach. In Solar to

Chemical Energy Conversion, M. Sugiyama, K. Fujii, and S. Nakamura, eds. (Springer International Publishing), pp. 191–211.

19. Kuhl, K.P., Hatsukade, T., Cave, E.R., Abram, D.N., Kibsgaard, J., and Jaramillo, T.F. (2014). Electrocatalytic conversion of carbon dioxide to methane and methanol on transition metal surfaces. J. Am. Chem. Soc. *136*, 14107–14113.

20. Zheng, Y., Jiao, Y., Jaroniec, M., and Qiao, S.Z. (2015). Advancing the electrochemistry of the hydrogen-evolution reaction through combining experiment and theory. Angew. Chem. Int. Ed. *54*, 52–65.

21. Lv, H.F., Li, D.G., Strmcnik, D., Paulikas, A.P., Markovic, N.M., and Stamenkovic, V.R. (2016). Recent advances in the design of tailored nanomaterials for efficient oxygen reduction reaction. Nano Energy *29*, 149–165.

22. Nie, Y., Li, L., and Wei, Z. (2015). Recent advancements in Pt and Pt-free catalysts for oxygen reduction reaction. Chem. Soc. Rev. *44*, 2168–2201.

23. Shao, M., Chang, Q., Dodelet, J.P., and Chenitz, R. (2016). Recent advances in electrocatalysts for oxygen reduction reaction. Chem. Rev. *116*, 3594–3657.

24. Huang, X.Q., Zhao, Z.P., Cao, L., Chen, Y., Zhu, E.B., Lin, Z.Y., Li, M.F., Yan, A.M., Zettl, A., Wang, Y.M., et al. (2015). High-performance transition metal-doped Pt_3Ni octahedra for oxygen reduction reaction. Science *348*, 1230–1234.

25. Stamenkovic, V.R., Fowler, B., Mun, B.S., Wang, G., Ross, P.N., Lucas, C.A., and Markovic, N.M. (2007). Improved oxygen reduction activity on $Pt_3Ni(111)$ via increased surface site availability. Science *315*, 493–497.

26. Hori, Y., Takahashi, I., Koga, O., and Hoshi, N. (2002). Selective formation of C2 compounds from electrochemical reduction of CO_2 at a series of copper single crystal electrodes. J. Phys. Chem. B *106*, 15–17.

27. Hori, Y., Kikuchi, K., Murata, A., and Suzuki, S. (1986). Production of methane and ethylene in electrochemical reduction of carbon dioxide at copper electrode in aqueous hydrogen carbonate solution. Chem. Lett. *15*, 897–898.

28. Schouten, K.J.P., Kwon, Y., van der Ham, C.J.M., Qin, Z., and Koper, M.T.M. (2011). A new mechanism for the selectivity to C_1 and C_2 species in the electrochemical reduction of carbon dioxide on copper electrodes. Chem. Sci. *2*, 1902–1909.

29. Hori, Y., Murata, A., and Takahashi, R. (1989). Formation of hydrocarbons in the electrochemical reduction of carbon dioxide at a copper electrode in aqueous solution. J. Chem. Soc. Faraday Trans. 1 *85*, 2309–2326.

30. Jovanov, Z.P., Hansen, H.A., Varela, A.S., Malacrida, P., Peterson, A.A., Norskov, J.K., Stephens, I.E.L., and Chorkendorff, I. (2016). Opportunities and challenges in the electrocatalysis of CO_2 and CO reduction using bifunctional surfaces: a theoretical and experimental study of Au-Cd alloys. J. Catal. *343*, 215–231.

31. Hashiba, H., Sato, H.K., Yotsuhashi, S., Fujii, K., Sugiyama, M., and Nakano, Y. (2017). A broad parameter range for selective methane production with bicarbonate solution in electrochemical CO_2 reduction. Sustain. Energy Fuels *1*, 1734–1739.

32. Durand, W.J., Peterson, A.A., Studt, F., Abild-Pedersen, F., and Norskov, J.K. (2011). Structure effects on the energetics of the electrochemical reduction of CO_2 by copper surfaces. Surf. Sci. *605*, 1354–1359.

33. Hansen, H.A., Shi, C., Lausche, A.C., Peterson, A.A., and Norskov, J.K. (2016). Bifunctional alloys for the electroreduction of CO_2 and CO. Phys. Chem. Chem. Phys. *18*, 9194–9201.

34. Peterson, A.A., Abild-Pedersen, F., Studt, F., Rossmeisl, J., and Norskov, J.K. (2010). How copper catalyzes the electroreduction of carbon dioxide into hydrocarbon fuels. Energy Environ. Sci. *3*, 1311–1315.

35. Nie, X., Esopi, M.R., Janik, M.J., and Asthagiri, A. (2013). Selectivity of CO_2 reduction on copper electrodes: the role of the kinetics of elementary steps. Angew. Chem. Int. Ed. *52*, 2459–2462.

36. Nie, X.W., Luo, W.J., Janik, M.J., and Asthagiri, A. (2014). Reaction mechanisms of CO_2 electrochemical reduction on Cu(111) determined with density functional theory. J. Catal. *312*, 108–122.

37. Ulissi, Z.W., Tang, M.T., Xiao, J.P., Liu, X.Y., Torelli, D.A., Karamad, M., Cummins, K., Hahn, C., Lewis, N.S., Jaramillo, T.F., et al. (2017). Machine-learning methods enable exhaustive searches for active bimetallic facets and reveal active site motifs for CO_2 reduction. ACS Catal. *7*, 6600–6608.

38. Abild-Pedersen, F., Greeley, J., Studt, F., Rossmeisl, J., Munter, T.R., Moses, P.G., Skulason, E., Bligaard, T., and Norskov, J.K. (2007). Scaling properties of adsorption energies for hydrogen-containing molecules on transition-metal surfaces. Phys. Rev. Lett. *99*, 016105.

39. Li, Y.W., and Sun, Q. (2016). Recent advances in breaking scaling relations for effective electrochemical conversion of CO_2. Adv. Energy Mater. *6*, 1600463.

40. Zhu, W., Michalsky, R., Metin, O., Lv, H., Guo, S., Wright, C.J., Sun, X., Peterson, A.A., and Sun, S. (2013). Monodisperse Au nanoparticles for selective electrocatalytic reduction of CO_2 to CO. J. Am. Chem. Soc. *135*, 16833–16836.

41. Dutta, A., Rahaman, M., Luedi, N.C., and Broekmann, P. (2016). Morphology matters: tuning the product distribution of CO_2 electroreduction on oxide-derived Cu foam catalysts. ACS Catal. *6*, 3804–3814.

42. Raciti, D., Livi, K.J., and Wang, C. (2015). Highly dense Cu nanowires for low-overpotential CO_2 reduction. Nano Lett. *15*, 6829–6835.

43. Sen, S., Liu, D., and Palmore, G.T.R. (2014). Electrochemical reduction of CO_2 at copper nanofoams. ACS Catal. *4*, 3091–3095.

44. Wang, Z.L., Li, C.L., and Yamauchi, Y. (2016). Nanostructured nonprecious metal catalysts for electrochemical reduction of carbon dioxide. Nano Today *11*, 373–391.

45. He, J., Dettelbach, K.E., Salvatore, D.A., Li, T., and Berlinguette, C.P. (2017). High-throughput synthesis of mixed-metal electrocatalysts for CO_2 reduction. Angew. Chem. Int. Ed. *56*, 6068–6072.

46. Kim, D., Resasco, J., Yu, Y., Asiri, A.M., and Yang, P. (2014). Synergistic geometric and electronic effects for electrochemical reduction of carbon dioxide using gold-copper bimetallic nanoparticles. Nat. Commun. *5*, 4948.

47. Jiao, Y., Zheng, Y., Chen, P., Jaroniec, M., and Qiao, S.Z. (2017). Molecular scaffolding strategy with synergistic active centers to facilitate electrocatalytic CO_2 reduction to hydrocarbon/alcohol. J. Am. Chem. Soc. *139*, 18093–18100.

48. Norskov, J.K., Bligaard, T., Logadottir, A., Kitchin, J.R., Chen, J.G., Pandelov, S., and Norskov, J.K. (2005). Trends in the exchange current for hydrogen evolution. J. Electrochem. Soc. *152*, J23–J26.

49. Greeley, J., Stephens, I.E.L., Bondarenko, A.S., Johansson, T.P., Hansen, H.A., Jaramillo, T.F., Rossmeisl, J., Chorkendorff, I., and Nørskov, J.K. (2009). Alloys of platinum and early transition metals as oxygen reduction electrocatalysts. Nat. Chem. *1*, 552.

50. Trasatti, S. (1972). Work function, electronegativity, and electrochemical behaviour of metals: III. Electrolytic hydrogen evolution in acid solutions. J. Electroanal. Chem. *39*, 163–184.

51. Kepp, K.P. (2016). A quantitative scale of oxophilicity and thiophilicity. Inorg. Chem. *55*, 9461–9470.

52. Christophe, J., Doneux, T., and Buess-Herman, C. (2012). Electroreduction of carbon dioxide on copper-based electrodes: activity of copper single crystals and copper-gold alloys. Electrocatalysis *3*, 139–146.

53. Jia, F.L., Yu, X.X., and Zhang, L.Z. (2014). Enhanced selectivity for the electrochemical reduction of CO_2 to alcohols in aqueous solution with nanostructured Cu-Au alloy as catalyst. J. Power Sources *252*, 85–89.

54. Kim, D., Xie, C., Becknell, N., Yu, Y., Karamad, M., Chan, K., Crumlin, E.J., Norskov, J.K., and Yang, P. (2017). Electrochemical activation of CO_2 through atomic ordering transformations of AuCu nanoparticles. J. Am. Chem. Soc. *139*, 8329–8336.

55. Ross, M.B., Dinh, C.T., Li, Y., Kim, D., De Luna, P., Sargent, E.H., and Yang, P. (2017). Tunable Cu enrichment enables designer syngas electrosynthesis from CO_2. J. Am. Chem. Soc. *139*, 9359–9363.

56. Monzo, J., Malewski, Y., Kortlever, R., Vidal-Iglesias, F.J., Solla-Gullon, J., Koper, M.T.M., and Rodriguez, P. (2015). Enhanced electrocatalytic activity of Au@Cu core@shell nanoparticles towards CO2 reduction. J. Mater. Chem. A *3*, 23690–23698.

57. Shi, C., Hansen, H.A., Lausche, A.C., and Norskov, J.K. (2014). Trends in electrochemical CO_2 reduction activity for

open and close-packed metal surfaces. Phys. Chem. Chem. Phys. *16*, 4720–4727.

58. Chen, K., Zhang, X., Williams, T., Bourgeois, L., and MacFarlane, D.R. (2017). Electrochemical reduction of CO_2 on core-shell Cu/Au nanostructure arrays for syngas production. Electrochim. Acta *239*, 84–89.

59. Chang, Z.Y., Huo, S.J., Zhang, W., Fang, J.H., and Wang, H.L. (2017). The tunable and highly selective reduction products on Ag@Cu bimetallic catalysts toward CO_2 electrochemical reduction reaction. J. Phys. Chem. C *121*, 11368–11379.

60. Choi, J., Kim, M.J., Ahn, S.H., Choi, I., Jang, J.H., Ham, Y.S., Kim, J.J., and Kim, S.-K. (2016). Electrochemical CO_2 reduction to CO on dendritic Ag-Cu electrocatalysts prepared by electrodeposition. Chem. Eng. J. *299*, 37–44.

61. Gurudayal, Bullock, J., Sranko, D.F., Towle, C.M., Lum, Y.W., Hettick, M., Scott, M.C., Javey, A., and Ager, J. (2017). Efficient solar-driven electrochemical CO_2 reduction to hydrocarbons and oxygenates. Energy Environ. Sci. *10*, 2222–2230.

62. Clark, E.L., Hahn, C., Jaramillo, T.F., and Bell, A.T. (2017). Electrochemical CO_2 reduction over compressively strained CuAg surface alloys with enhanced multi-carbon oxygenate selectivity. J. Am. Chem. Soc. *139*, 15848–15857.

63. Ren, D., Ang, B.S.H., and Yeo, B.S. (2016). Tuning the selectivity of carbon dioxide electroreduction toward ethanol on oxide-derived Cu_xZn catalysts. ACS Catal. *6*, 8239–8247.

64. Hori, Y., Murata, A., and Ito, S.-Y. (1990). Enhanced evolution of CO and suppressed formation of hydrocarbons in electroreduction of CO_2 at a copper electrode modified with cadmium. Chem. Lett. *19*, 1231–1234.

65. Lv, W., Zhang, R., Gao, P., and Lei, L. (2014). Studies on the faradaic efficiency for electrochemical reduction of carbon dioxide to formate on tin electrode. J. Power Sources *253*, 276–281.

66. Morimoto, M., Takatsuji, Y., Yamasaki, R., Hashimoto, H., Nakata, I., Sakakura, T., and Haruyama, T. (2017). Electrodeposited Cu-Sn alloy for electrochemical CO_2 reduction to $CO/HCOO^-$. Electrocatalysis *8*, 1–10.

67. Sarfraz, S., Garcia-Esparza, A.T., Jedidi, A., Cavallo, L., and Takanabe, K. (2016). Cu-Sn bimetallic catalyst for selective aqueous electroreduction of CO_2 to CO. ACS Catal. *6*, 2842–2851.

68. Li, Q., Fu, J., Zhu, W., Chen, Z., Shen, B., Wu, L., Xi, Z., Wang, T., Lu, G., Zhu, J.J., and Sun, S. (2017). Tuning Sn-catalysis for electrochemical reduction of CO_2 to CO via the core/shell Cu/SnO_2 structure. J. Am. Chem. Soc. *139*, 4290–4293.

69. Schreier, M., Heroguel, F., Steier, L., Ahmad, S., Luterbacher, J.S., Mayer, M.T., Luo, J.S., and Gratzel, M. (2017). Solar conversion of CO_2 to CO using Earth-abundant electrocatalysts prepared by atomic layer modification of CuO. Nat. Energy *2*, 17087.

70. Rasul, S., Anjum, D.H., Jedidi, A., Minenkov, Y., Cavallo, L., and Takanabe, K. (2015). A highly selective copper-indium bimetallic electrocatalyst for the electrochemical reduction of aqueous CO_2 to CO. Angew. Chem. Int. Ed. *54*, 2146–2150.

71. Martin, R., and Buchwald, S.L. (2008). Palladium-catalyzed Suzuki-Miyaura cross-coupling reactions employing dialkylbiaryl phosphine ligands. Acc. Chem. Res. *41*, 1461–1473.

72. Suh, D.J., Park, T.J., and Ihm, S.K. (1992). Characteristics of carbon-supported palladium catalysts for liquid-phase hydrogenation of nitroaromatics. Ind. Eng. Chem. Res. *31*, 1849–1856.

73. Conrad, H., Ertl, G., and Latta, E.E. (1974). Adsorption of hydrogen on palladium single-crystal surfaces. Surf. Sci. *41*, 435–446.

74. Jewell, L.L., and Davis, B.H. (2006). Review of absorption and adsorption in the hydrogen-palladium system. Appl. Catal. A *310*, 1–15.

75. Kyriakou, G., Boucher, M.B., Jewell, A.D., Lewis, E.A., Lawton, T.J., Baber, A.E., Tierney, H.L., Flytzani-Stephanopoulos, M., and Sykes, E.C.H. (2012). Isolated metal atom geometries as a strategy for selective heterogeneous hydrogenations. Science *335*, 1209–1212.

76. Bai, S., Shao, Q., Wang, P., Dai, Q., Wang, X., and Huang, X. (2017). Highly active and selective hydrogenation of CO_2 to ethanol by ordered Pd-Cu nanoparticles. J. Am. Chem. Soc. *139*, 6827–6830.

77. Li, M., Wang, J.J., Li, P., Chang, K., Li, C.L., Wang, T., Jiang, B., Zhang, H.B., Liu, H.M., Yamauchi, Y., et al. (2016). Mesoporous palladium-copper bimetallic electrodes for selective electrocatalytic reduction of aqueous CO_2 to CO. J. Mater. Chem. A *4*, 4776–4782.

78. Li, M., Li, P., Chang, K., Liu, H., Hai, X., Zhang, H., and Ye, J. (2016). Design of a photoelectrochemical device for the selective conversion of aqueous CO_2 to CO: using mesoporous palladium-copper bimetallic cathode and hierarchical ZnO-based nanowire array photoanode. Chem. Commun. *52*, 8235–8238.

79. Takashima, T., Suzuki, T., and Irie, H. (2017). Electrochemical carbon dioxide reduction on copper-modified palladium nanoparticles synthesized by underpotential deposition. Electrochim. Acta *229*, 415–421.

80. Hammer, B., Morikawa, Y., and Norskov, J.K. (1996). CO chemisorption at metal surfaces and overlayers. Phys. Rev. Lett. *76*, 2141–2144.

81. Ma, S., Sadakiyo, M., Heima, M., Luo, R., Haasch, R.T., Gold, J.I., Yamauchi, M., and Kenis, P.J. (2017). Electroreduction of carbon dioxide to hydrocarbons using bimetallic Cu-Pd catalysts with different mixing patterns. J. Am. Chem. Soc. *139*, 47–50.

82. Long, R., Li, Y., Liu, Y., Chen, S., Zheng, X., Gao, C., He, C., Chen, N., Qi, Z., Song, L., et al. (2017). Isolation of Cu atoms in Pd lattice: forming highly selective sites for photocatalytic conversion of CO_2 to CH_4. J. Am. Chem. Soc. *139*, 4486–4492.

83. Varela, A.S., Schlaup, C., Jovanov, Z.P., Malacrida, P., Horch, S., Stephens, I.E.L., and Chorkendorff, I. (2013). CO_2 electroreduction on well-defined bimetallic surfaces: Cu overlayers on Pt(111) and Pt(211). J. Phys. Chem. C *117*, 20500–20508.

84. Guo, X., Zhang, Y., Deng, C., Li, X., Xue, Y., Yan, Y.M., and Sun, K. (2015). Composition dependent activity of Cu-Pt nanocrystals for electrochemical reduction of CO_2. Chem. Commun. *51*, 1345–1348.

85. Ko, J., Kim, B.K., and Han, J.W. (2016). Density functional theory study for catalytic activation and dissociation of CO_2 on bimetallic alloy surfaces. J. Phys. Chem. C *120*, 3438–3447.

86. Back, S., Yeom, M.S., and Jung, Y. (2015). Active sites of Au and Ag nanoparticle catalysts for CO_2 electroreduction to CO. ACS Catal. *5*, 5089–5096.

87. Back, S., Kim, J.H., Kim, Y.T., and Jung, Y. (2016). Bifunctional interface of Au and Cu for improved CO_2 electroreduction. ACS Appl. Mater. Interfaces *8*, 23022–23027.

88. Han, B.C., Miranda, C.R., and Ceder, G. (2008). Effect of particle size and surface structure on adsorption of O and OH on platinum nanoparticles: a first-principles study. Phys. Rev. B Condens. Matter Mater. Phys. *77*, 075410.

89. Hirunsit, P., Soodsawang, W., and Limtrakul, J. (2015). CO_2 electrochemical reduction to methane and methanol on copper-based alloys: theoretical insight. J. Phys. Chem. C *119*, 8238–8249.

90. Adit Maark, T., and Nanda, B.R.K. (2016). CO and CO_2 electrochemical reduction to methane on Cu, Ni, and Cu_3Ni (211) surfaces. J. Phys. Chem. C *120*, 8781–8789.

91. Adit Maark, T., and Nanda, B.R.K. (2017). Enhancing CO_2 electroreduction by tailoring strain and ligand effects in bimetallic copper-rhodium and copper-nickel heterostructures. J. Phys. Chem. C *121*, 4496–4504.

92. Liu, M., Pang, Y., Zhang, B., De Luna, P., Voznyy, O., Xu, J., Zheng, X., Dinh, C.T., Fan, F., Cao, C., et al. (2016). Enhanced electrocatalytic CO_2 reduction via field-induced reagent concentration. Nature *537*, 382–386.

93. Resasco, J., Chen, L.D., Clark, E., Tsai, C., Hahn, C., Jaramillo, T.F., Chan, K., and Bell, A.T. (2017). Promoter effects of alkali metal cations on the electrochemical reduction of carbon dioxide. J. Am. Chem. Soc. *139*, 11277–11287.

94. Singh, M.R., Kwon, Y., Lum, Y., Ager, J.W., 3rd, and Bell, A.T. (2016). Hydrolysis of electrolyte cations enhances the electrochemical reduction of CO_2 over Ag and Cu. J. Am. Chem. Soc. *138*, 13006–13012.

95. Zhao, W.G., Yang, L.N., Yin, Y.D., and Jin, M.S. (2014). Thermodynamic controlled synthesis of intermetallic Au_3Cu alloy nanocrystals from Cu microparticles. J. Mater. Chem. A *2*, 902–906.

96. Weng, Z., Zhang, X., Wu, Y., Huo, S., Jiang, J., Liu, W., He, G., Liang, Y., and Wang, H. (2017). Self-cleaning catalyst electrodes for stabilized

CO_2 reduction to hydrocarbons. Angew. Chem. Int. Ed. *56*, 13135–13139.

97. Zhang, S., Kang, P., Bakir, M., Lapides, A.M., Dares, C.J., and Meyer, T.J. (2015). Polymer-supported CuPd nanoalloy as a synergistic catalyst for electrocatalytic reduction of carbon dioxide to methane. Proc. Natl. Acad. Sci. USA *112*, 15809–15814.

98. Chen, C.S., Wan, J.H., and Yeo, B.S. (2015). Electrochemical reduction of carbon dioxide to ethane using nanostructured Cu_2O-derived copper catalyst and palladium(II) chloride. J. Phys. Chem. C *119*, 26875–26882.

99. Kaneco, S., Sakaguchi, Y., Katsumata, H., Suzuki, T., and Ohta, K. (2007). Cu-deposited nickel electrode for the electrochemical conversion of CO_2 in water/methanol mixture media. Bull. Catal. Soc. India *6*, 74–82.

100. Li, Y.W., Su, H.B., Chan, S.H., and Sun, Q. (2015). CO_2 electroreduction performance of transition metal dimers supported on graphene: a theoretical study. ACS Catal. *5*, 6658–6664.